Inorganic Chemistry

ARTICLE

pubs.acs.org/IC

Bioinspired Systems for Metal-Ion Sensing: New Emissive Peptide Probes Based on Benzo[*d*]oxazole Derivatives and Their Gold and Silica Nanoparticles[||]

Elisabete Oliveira,[†,‡] Damiano Genovese,[§] Riccardo Juris,[§] Nelsi Zaccheroni,[§] José Luis Capelo,[†,‡] M. Manuela M. Raposo,[⊥] Susana P. G. Costa,[*,⊥] Luca Prodi,[*,§] and Carlos Lodeiro[*,†,‡]

[†]REQUIMTE, Department of Chemistry, FCT-UNL, 2829-516 Monte de Caparica, Portugal

[‡]BIOSCOPE Group, Faculty of Science, Physical Chemistry Department, University of Vigo, Campus Ourense, 32004 Ourense, Spain

[§]Department of Chemistry "G. Ciamician", Università degli Studi di Bologna, 40126 Bologna, Italy

[⊥]CQ-UM, Center of Chemistry, University of Minho, Campus Gualtar, 4710-057 Braga, Portugal

Supporting Information

ABSTRACT: Seven new bioinspired chemosensors (**2**−**4** and **7**−**10**) based on fluorescent peptides were synthesized and characterized by elemental analysis, ^{1}H and ^{13}C NMR, melting point, matrix-assisted laser desorption−ionization time-of-flight mass spectrometry (MALDI-TOF-MS), and IR and UV−vis absorption and emission spectroscopy. The interaction with transition- and post-transition-metal ions (Cu^{2+}, Ni^{2+}, Ag^{+}, Zn^{2+}, Cd^{2+}, Hg^{2+}, Pb^{2+}, and Fe^{3+}) has been explored by absorption and fluorescence emission spectroscopy and MALDI-TOF-MS. The reported fluorescent peptide systems, introducing biological molecules in the skeleton of the probes, enhance their sensitivity and confer them strong potential for applications in biological fields. Gold and silica nanoparticles functionalized with these peptides were also obtained. All nanoparticles were characterized by dynamic light scattering, transmission electron microscopy, and UV−vis absorption and fluorescence spectroscopy. Stable gold nanoparticles (diameter 2−10 nm) bearing ligands **1** and **4** were obtained by common reductive synthesis. Commercial silica nanoparticles were decorated at their surface using compounds **8**−**10**, linked through a silane spacer. The same chemosensors were also taken into aqueous solutions through their dispersion in the outer layer of silica core/poly(ethylene glycol) shell nanoparticles. In both cases, these complex nanoarchitectures behaved as new sensitive materials for Ag^{+} and Hg^{2+} in water. The possibility of using these species in this solvent is particularly valuable because the impact on human health of heavy- and transition-metal-ion pollution is very severe, and all analytical and diagnostics investigations involve a water environment.

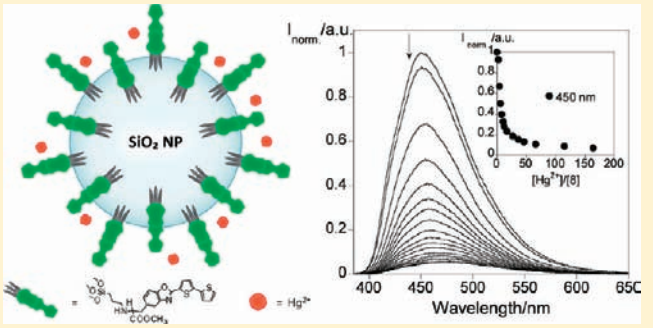

INTRODUCTION

Fluorescent chemosensors have experienced a great development in the last decades because of their important applications in many different areas, in particular in medical diagnostics, environmental control, and material sciences.[1] In a conjugate chemosensor, three main structural components can be distinguished: (i) the receptor, (ii) the fluorophore, and, in some cases, (iii) the spacer. In this framework, bioinspired systems, i.e., chemosensors in which the binding moiety is a natural or synthetic amino acid or a peptide chain, are particularly valuable and suitable for applications both in biotechnology and in nanoelectronics.[2] Wiczk and co-workers have presented several examples of alanine derivatives for metal-ion detection[3] in which the introduction of a peptide chain is fundamental for the recognition event. Histidine, glutamine, and cysteine are known to be the specific binding residues for Zn^{2+} in enzymes, while proline and glycine induce the bending of the structure, ensuring preorganization of the system. Lee and co-workers have merged these two aspects by synthesizing a short peptide probe bound to a dansyl fluorophore to yield a selective chemosensor for extracellular and environmental zinc.[4] Andreopoulos, Leblanc, and collaborators[5] have, in turn, shown that the selectivity of short peptidyl sequences toward metal cations and, in particular, toward Cu^{2+} ions, was greatly influenced by the reciprocal spatial alignment of the fluorophore and the amino acidic binding chain. The different arrangements of the various units in the chemosensor induced different transduction mechanisms between the receptor and the signaling dansyl group, which resulted in a different sensing performance.[5] On the other hand, Yang and Li investigated the possibilities offered by a long and flexible architecture by preparing a luminescent chemosensor for metal ions in aqueous solution based on the conjugation of amino acids with multidentate aminocarboxylate ligands.[6] In this case, the

Received: April 18, 2011
Published: August 17, 2011

Scheme 1. Synthesis of Peptides and Precursors

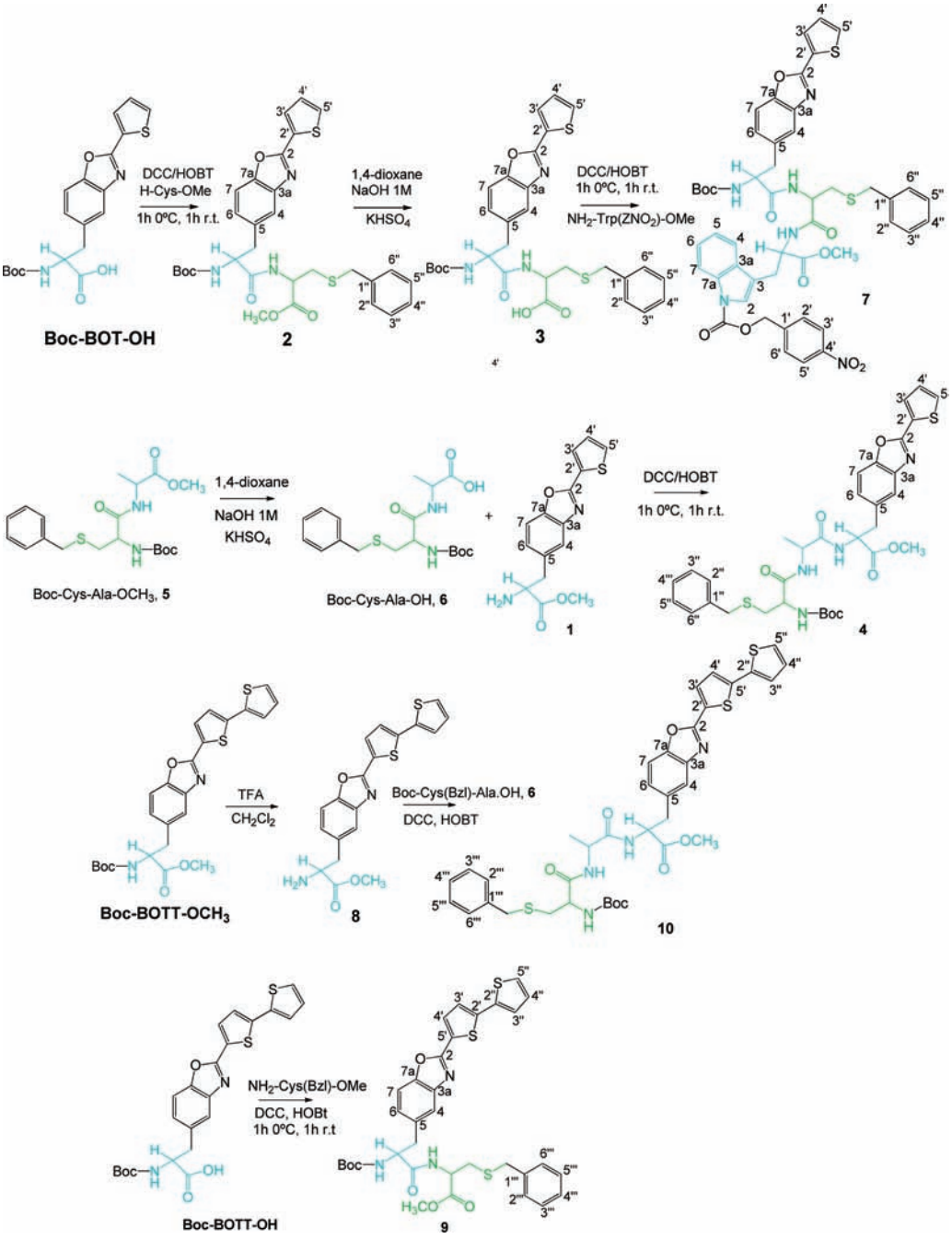

system presented an ethylenediaminetetraacetic acid derivative functionalized with two tryptophans, whose indole moiety represented the signaling units, being also involved in the recognition event. This species revealed a remarkable selectivity for Ca^{2+} over other mono- and divalent cations in water, as shown by an important enhancement of the fluorescence intensity.

Peptide derivatives containing benzoxazole units as chromophores are also known. Benzoxazoles have important biological applications as inhibitors of human cysteine proteases, as ligands of the *N*-metil D-aspartato receptor, and as biomarkers or biosensors.[7]

Recently, however, research is moving toward more complex and sophisticated structures, trying to push further their limits of sensitivity and selectivity. Many different solutions have been proposed, but among them, sensing systems based on nanoparticles are certainly some of the most interesting and promising.[8] The impressive huge range of interests and applications of nanoparticles arises from the incredible versatility and modulation of their properties. A great number of materials can be used to engineer nanoparticles such as carbon (fullerenes, carbon dots, etc.), metals (silver, gold, copper, and platinum), metal oxides (zinc, iron, titanium, and copper oxides), semiconductors (e.g., CdSe/ZnS, PbS, InGaP, called quantum dots), silica, polymers,

dx.doi.org/10.1021/ic200792t |*Inorg. Chem.* 2011, 50, 8834–8849

surfactants, lipids, and many different mixtures of two or more of them. Moreover, it is possible, in many cases, to derivatize their surface with different capping agents (receptors, chemosensors, DNA strains, etc.) to introduce whatever functionality is desired.[9] Among the different nanoparticles listed above, properly modified gold nanoparticles (AuNPs) and silica nanoparticles can be seen as very interesting options for solving important analytical problems including those related to medical diagnosis and imaging.

Gold nanoclusters, even if already known and used for their iridescent colors since centuries before Christ, have gained great importance only in the last decades in biology and medicine: their possible applications when functionalized with biomolecules in sensing, diagnostics, and therapeutics are really outstanding.[10,11] In this context, a new generation of sensing materials using soft donor atoms such as sulfur has been used for decorating AuNPs.[1,9,12,13]

On the other hand, because of the favorable chemical, optical, and toxicological properties of silica,[14] the incorporation of fluorescent chemosensors in monodisperse silica nanoparticles yielded a new group of fluorescent materials with improved properties, such as higher affinity, versatility, and sensitivity, also due in some cases to signal amplification processes.[15]

Although some examples of decorated nanoparticles with peptides have been reported recently for heavy-metal-ion detection,[16] this is the first time in which highly fluorescent (oligo)thienylbenzo[*d*]oxazole derivatives have been incorporated as fluorophores into emissive nanoparticle devices.

Following our ongoing research project on bioinspired fluorescent chemosensors using amino acids as building blocks, we have already explored thiophene and bithiophene rings as new sulfur-donor chelating units within an amino acid core.[17] The resulting highly fluorescent unnatural heterocyclic alanine derivatives (Φ_F = 0.26−0.80) showed a noticeable quenching upon complexation with paramagnetic Fe^{3+}, Cu^{2+}, and Ni^{2+} metal ions and with diamagnetic Hg^{2+} ions. A negligible interaction with other important biological metal ions such as Zn^{2+}, Ca^{2+}, and Na^+ was also observed.[17]

Among all of the transition and post-transition metal ions, detection of Hg^{2+} and Ag^+ is very important because of their environmental effects. Hg^{2+} is the most toxic of the hard metal ions and normally shows complex and uncommon chemical and physical properties; on the other hand, Ag^+ has received considerable attention because of its bioaccumulation effects and antimicrobial activity. These properties are at the basis of the continuosly increasing interest for the development of new fluorescent chemosensors for both of these metal ions.[18,19]

In the present paper, we report the synthesis of seven new emissive peptide-based compounds, **2**−**4** and **7**−**10**, containing alanine, cysteine, or tryptophan as building blocks, combined with two synthetic amino acids, [2-(thien-2′-yl)benzo[*d*]oxazol-5-yl]-L-alanine (BOT) and [2-(bithien-2′-yl)benzo[*d*]oxazol-5-yl]-L-alanine (BOTT) (Scheme 1). The (oligo)thienylbenzo[*d*]oxazole chromophore was used as an emissive unit in all cases. All compounds were characterized by elemental analysis, melting point, matrix-assisted laser desorption−ionization time-of-flight mass spectrometry (MALDI-TOF-MS), IR, UV−vis absorption, fluorescence emission, and ^{1}H and ^{13}C NMR spectroscopy. Their interaction with several mono- and divalent metal ions was followed by spectroscopic techniques. AuNPs and silica nanoparticles decorated with these new peptides were synthesized and characterized by fluorescence spectroscopy, dynamic light scattering (DLS), and transmission electron microscopy (TEM). The complexation ability of the silica nanoparticles in solution was also investigated. Our purpose was to explore the possibility of using these biocompatible compounds supported on different surfaces to verify whether their characteristics and properties would have been maintained or even improved.

With this goal in mind we used our biosensing moieties to decorate the surface of AuNPs and silica nanoparticles and then water micelles of Pluronic F127 shell nanoparticles.

EXPERIMENTAL SECTION

Chemicals and Starting Reagents. Solvents and starting materials were purchased from commercial sources where available and used without further purifications if not otherwise specified. $Cu(CF_3SO_3)_2\cdot xH_2O$, $Ni(BF_4)_2\cdot 6H_2O$, $Ag(BF_4)\cdot xH_2O$, $Zn(CF_3SO_3)_2\cdot xH_2O$, $Cd(ClO_4)_2\cdot 6H_2O$, $Hg(CF_3SO_3)_2\cdot xH_2O$, $Pb(CF_3SO_3)_2\cdot xH_2O$, and $Fe(NO_3)_3\cdot 6H_2O$ salts have been purchased from Strem Chemicals, Sigma Aldrich, and Solchemar. Thionyl chloride, *N*,*N*′-dicyclohexylcarbodiimide (DCC), Boc-Cys(Bzl)-OH, and NH_2-Trp(ZNO_2)-OMe were purchased from Fluka. 1-Hydroxybenzotriazole (HOBt) was purchased from Senn Chemicals. Triethylamine, sodium hydroxide, anhydrous sodium sulfate, dithiobis(succinimidylpropionate) (DSP), tetraoctylammonium bromide (TOAB), L-alanine, $HAuCl_4$, $NaBH_4$, and trifluoracetic acid (TFA) and all of the solvents used were from Sigma Aldrich. $KHSO_4$ and silica gel for chromatography were from Merck. The silica nanoparticles that we have used are Ludox AS-30 by Sigma-Aldrich (with a diameter of 15 ± 3 nm measured by TEM and a hydrodynamic diameter of 20 ± 3 nm obtained by DLS). Water was always used purified and deionized (Milli-Q grade, Millipore).

Synthesis of Peptides. The synthesis and characterization of the parent compounds **1**, Boc-BOT-OH, Boc-BOTT-OCH_3, and Boc-BOTT-OH were previously described (see Scheme 1).[17a,b]

*1. Synthesis of Boc-BOT-Cys(Bzl)-OMe (**2**).* Boc-BOT-OH[17] (0.13 g, 3.26×10^{-4} mol) was dissolved in distilled dimethylformamide (DMF; 2 mL) cooled in an ice bath, followed by the addition of HOBt (0.04 g, 3.26×10^{-4} mol) and DCC (0.07 g, 3.26×10^{-4} mol), and this mixture was stirred in an ice bath for 30 min.

In a separate flask, thionyl chloride (0.20 mL, 2.60×10^{-2} mol) was added dropwise with stirring to methanol (10 mL) cooled in an ice bath, followed by the addition of Boc-Cys(Bzl)-OH (0.81 g, 2.60×10^{-2} mol). The solution was refluxed at boiling temperature for 2 h. The solvent was evaporated under reduced pressure, yielding an oil. The oil was triturated with diethyl ether, leading to a white solid (HCl·H-Cys-OMe).

In a next step, HCl·H-Cys-OMe (0.09 g, 3.26×10^{-4} mol) was neutralized with triethylamine (43 μL, 3.26×10^{-4} mol) in distilled DMF for 30 min. The solution was filtered and added to the solution containing Boc-BOT-OH. The final mixture was stirred for 1 h in an ice bath and 1 h at room temperature. The solvent was evaporated under reduced pressure, and the residue was treated with cooled acetone to remove *N*,*N*′-dicyclohexylurea (DCU) through filtration. The solvent was evaporated, and the residue was purified by column chromatography with silica gel (eluent: 100:1 and 100:2 CH_2Cl_2/MeOH). The fractions were combined, and the product **2** was obtained as a yellow solid (0.14 g, 75%): mp 94−97 °C, $C_{30}H_{33}N_3O_6S_2\cdot{}^3/_2CH_3CH_2OCH_2CH_3$, fw = 706.9. Elem anal. Calcd: C, 61.2; H, 6.8; N, 6.0; S, 9.1. Found: C, 61.4; H, 6.6; N, 6.3; S, 9.4.

NMR Data. ^{1}H NMR ($CDCl_3$, 300 MHz): δ 1.41 (s, 9H, $C(CH_3)_3$), 2.74−2.94 (m, 2H, β-CH_2Cys), 3.19 (d, *J* = 6.3 Hz, 2H, β-CH_2 BOT), 3.65 (s, 2H, CH_2 Bzl), 3.70 (s, 3H, OCH_3), 4.42 (m, 1H, α-H Cys), 4.72−4.78 (m, 1H, α-H BOT), 5.00 (d, *J* = 5.7 Hz, 1H, NH BOT), 6.62 (d, *J* = 7.5 Hz, 1H, NH Cys), 7.18−7.30 (m, 7H, 5 × Ph−*H*, H6 and H4′), 7.45 (d, *J* = 8.4 Hz, 1H, H7), 7.55 (d, *J* = 1.2 Hz, 1H, H4), 7.57 (dd, *J* = 1.2 and 5.1 Hz, 1H, H5′), 7.91 (dd, *J* = 1.2 and 2.4 Hz, 1H, H3′).

^{13}C NMR ($CDCl_3$, 75.4 MHz): δ 28.26 (C($\underline{C}H_3)_3$), 33.40 (β-CH_2 Cys), 36.49 (CH_2 Bzl), 37.65 (β-CH_2 BOT), 52.40 (OCH_3), 53.41 (α-C Cys), 53.85 (α-C BOT), 80.05 ($\underline{C}(CH_3)_3$), 110.53 (C7), 119.73 (C4), 127.02 (C4″), 126.68 (C6), 128.55 (C2″ and C6″), 128.62 (C4′), 128.77 (C2), 128.97 (C3″ and C5″), 130.51 (C3′), 131.22 (C5′), 133.08 (C5), 138.12 (C1″), 141.14 (C3a), 149.17 (C7a), 155.28 (C═O Boc), 159.55 (C2′), 170.87 (C═O BOT), 171.00 (C═O Cys).

IR (NaCl windows, cm^{-1}): ν(NH st) 3300, ν(COO^- st) 1730, ν(C═O) 1696, ν(C═C benzene) 1663, ν($-CH_2$ δ) 1453, ν($-CH_3$ δ) 1369, ν(thiophene) 3061 (CH st), 1534 (CH γ), 746 (CH δ_{oop}).

MALDI-TOF-MS [calcd (found)]: $[\mathbf{2}H]^+$, 596.7 (596.5), 25%; $[\mathbf{2}H\cdot 5H_2O]^+$, 686.7 (686.4), 68%; $[\mathbf{2}\text{-BocH}]^+$, 496.6 (496.4), 40%; $[C_{11}H_7NOSNa]^+$, 225 (225.6), 100%.

*2. Synthesis of Boc-BOT-Cys(Bzl)-OH (**3**).* The precursor **2** (0.14 g, 2.43×10^{-4} mol) was dissolved in 1,4-dioxane (1 mL) in an ice bath, and a 1 M sodium hydroxide aqueous solution (0.36 mL, 1.5 equiv, 3.65×10^{-4} M) was added dropwise. The mixture was stirred at room temperature for 3 h. The pH was adjusted to 2−3 by the addition of a 1 M $KHSO_4$ aqueous solution and extracted with ethyl acetate (3 × 10 mL). After drying with anhydrous sodium sulfate, the solvent was evaporated under reduced pressure, and the residue was triturated with diethyl ether, yielding a white solid (0.10 g, 71%): mp 149−151 °C, $C_{29}H_{31}N_3O_6S_2$, fw = 581.7. Elem anal. Calcd: C, 59.9; H, 5.4; N, 7.2; S, 11.0. Found: C, 60.0; H, 5.6; N, 7.0; S, 10.8.

NMR Data. ^{1}H NMR (DMSO-d_6, 300 MHz): δ 1.24 (s, 9H, C($CH_3)_3$), 2.69−2.88 (m, 2H, β-CH_2 Cys), 3.09−3.15 (m, 2H, β-CH_2 BOT), 3.78 (s, 2H, CH_2 Bzl), 4.24−4.30 (m, 1H, α-H BOT), 4.45−4.51 (m, 1H, α-H Cys), 6.99 (d, J = 8.7 Hz, 1H, NH BOT), 7.22−7.36 (m, 7H, 5 × Ph−*H*, H6 and H4′), 7.63 (d, J = 8.7 Hz, 1H, H7), 7.66 (br s, 1H, H4), 7.92−7.95 (m, 2H, H3′ and H5′), 8.36 (d, J = 7.8 Hz, 1H, NH Cys).

^{13}C NMR (DMSO-d_6, 75.4 MHz): δ 28.22 (C($\underline{C}H_3)_3$), 32.23 (β-CH_2 Cys), 35.49 (CH_2 Bzl), 37.38 (β-CH_2 BOT), 52.00 (α-C Cys), 55.98 (α-C BOT), 78.05 ($\underline{C}(CH_3)_3$), 110.03 (C7), 120.14 (C4), 126.82 (C4″), 126.88 (C6), 128.37 (C3″ and C5″), 128.62 (C4′), 128.91 (C2), 128.98 (C2″ and C6″), 130.40 (C3′), 131.83 (C5′), 135.22 (C5), 138.24 (C1″), 141.34 (C3a), 148.69 (C7a), 155.26 (C═O Boc), 158.42 (C2′), 171.80 (C═O BOT), 172.00 (C═O Cys).

IR (NaCl windows, cm^{-1}): ν(NH st) 3300, ν(OH) 3423, ν(COO^- st) 1730, ν(C═O) 1696; ν(C═C benzene) 1663, ν($-CH_2$ δ) 1453, ν($-CH_3$ δ) 1369, ν(thiophene) 3061 (CH st), 1534 (CH γ), 746 (CH δ_{oop}).

MALDI-TOF-MS [calcd (found)]: $[\mathbf{3}H]^+$, 582.7 (582.5), 25%; $[\mathbf{3}\text{-BocH}]^+$, 482.6 (482.5), 5%; $[C_{11}H_7NOSNa]^+$, 225.0 (225.6), 100%.

*3. Synthesis of Boc-Cys(Bzl)-Ala-BOT-OMe (**4**).* This compound was synthesized in three steps, using compounds **5**, **6**, and **1** as precursors.

*Synthesis of Boc-Cys(Bzl)-Ala-OMe (**5**).* Thionyl chloride (2.5 mL, 3.40×10^{-2} mol) was added dropwise to stirring methanol (20 mL) in an ice bath, and then L-alanine (3 g, 3.36×10^{-2} mol) was added. The solution was refluxed at boiling temperature for 2 h. The solvent was evaporated under reduced pressure to obtain a brown solid. The crude mixture was washed with diethyl ether, yielding a white solid (HCl·H-Ala-OMe).

In a separate flask, Boc-Cys(Bzl)-OH (0.25 g, 8.03×10^{-4} mol) was dissolved in distilled DMF (2 mL) cooled in an ice bath, and then HOBt (0.11 g, 8.14×10^{-4} mol) and DCC (0.16 g, 7.75×10^{-4} mol) were added. The mixture was stirred in an ice bath for 30 min.

In a separate flask, HCl·H-Ala-OMe (0.11 g, 7.89×10^{-4} mol) was neutralized with triethylamine (0.11 mL, 8.03×10^{-4} mol) in distilled DMF for 30 min. The solution was filtered and then added to the solution containing the compound Boc-Cys(Bzl)-OH. The mixture was stirred 1 h in an ice bath and 1 h at room temperature. The solvent was evaporated under reduced pressure, and the residue was treated with cooled acetone to remove DCU through filtration. The solvent was evaporated, and the residue was purified by column chromatography with silica gel (eluent: $CHCl_3$). The fractions were combined, and the product **5** was obtained as a white solid (0.30 g, 87%): mp 93−95 °C, $C_{19}H_{28}N_2O_5S$, fw = 396.5 Elem anal. Calcd: C, 57.6; H, 7.1; N, 7.1; S, 8.1. Found: C, 57.6; H, 7.2; N, 7.0; S, 7.9.

NMR Data. ^{1}H NMR ($CDCl_3$, 400 MHz): δ 1.40 (d, J = 7.2 Hz, 3H, β-CH_3 Ala), 1.46 (s, 9H, C($CH_3)_3$), 2.76−2.78 (m, 1H, β-CH_2 Cys), 2.85−2.90 (m, 1H, β-CH_2 Cys), 3.74 (s, 3H, OCH_3), 3.75 (s, 2H, CH_2 Bzl), 4.22−4.27 (m, 1H, α-H Cys), 4.56 (m, 1H, α-H Ala), 5.30−5.35 (br s, 1H, NH Cys), 6.91 (d, J = 6.0 Hz, 1H, NH Ala), 7.31−7.34 (m, 5H, 5 × Ph−*H*).

^{13}C NMR ($CDCl_3$, 100 MHz): δ 18.25 (β-CH_3 Ala), 28.22 (C($\underline{C}H_3)_3$), 33.65 (β-CH_2 Cys), 36.45 (CH_2 Bzl), 48.19 (α-C Ala), 52.43 (OCH_3), 53.64 (α-C Cys), 80.32 ($\underline{C}(CH_3)_3$), 127.17 (C4″), 128.55 (C2″ and C6″), 128.97 (C3″ and C5″), 137.84 (C1″), 155.28 (C═O Boc), 170.16 (C═O Cys), 172.83 (C═O Ala).

*Synthesis of Boc-Cys(Bzl)-Ala-OH (**6**).* Compound **6** was obtained from **5** (0.21 g, 5.5×10^{-4} mol) through a procedure similar to that previously described for compound **3**: white solid (0.21 g, 87%), $C_{18}H_{26}N_2O_5S$, fw = 382.5. Elem anal. Calcd: C, 56.5; H, 6.8; N, 7.3; S, 8.4. Found: C, 56.6; H, 6.7; N, 7.4; S, 8.3.

NMR Data. ^{1}H NMR ($CDCl_3$, 300 MHz): δ 1.43 (s, 12H, C($CH_3)_3$ and β-CH_3 Ala), 2.75−2.78, (m, 2H, β-CH_2 Cys), 3.71 (s, 2H, CH_2 Bzl), 4.35−4.37 (br s, 1H, α-H Cys), 4.52−4.57 (m, 1H, α-H Ala), 5.62−5.65 (br s, 1H, NH Cys), 7.20−7.30 (m, 6H, 5 × Ph−*H* and NH Ala).

^{13}C NMR ($CDCl_3$, 75.4 MHz): δ 17.95 (β-CH_3 Ala), 28.10 (C($\underline{C}H_3)_3$), 33.50 (β-CH_2 Cys), 36.21 (CH_2 Bzl), 48.20 (α-C Ala), 53.48 (α-C Cys), 80.49 ($\underline{C}(CH_3)_3$), 127.03 (C4″), 128.42 (C2″ and C6″), 128.85 (C3″ and C5″), 137.64 (C1″), 155.67 (C═O Boc), 170.73 (C═O Cys), 175.08 (C═O Ala).

6 (0.19 g, 5.09×10^{-4} mol) was dissolved in distilled DMF (2 mL) in an ice bath, and then HOBt (0.08 g, 5.09×10^{-4} mol) and DCC (0.11 g, 5.09×10^{-4} mol) were added. The mixture was continuously stirred for 30 min before the ligand **1** (0.15 g, 5.09×10^{-4} mol) was added and then for another 2 h, 1 h at 0 °C and 1 h at room temperature. The solvent was evaporated under reduced pressure, and the residue was treated with cooled acetone to remove DCU through filtration. The solvent was evaporated, and the residue was purified by column chromatography with silica gel (eluent: 100:1 $CHCl_3$/MeOH). The fractions were combined, and the product **4** was obtained as a pale-orange solid (0.14 g, 42%): mp 140−142 °C, $C_{33}H_{38}N_4O_7S_2$, fw = 666.8. Elem anal. Calcd: C, 59.4; H, 5.7; N, 8.4; S, 9.6. Found: C, 59.6; H, 5.7; N, 8.4; S, 9.3.

NMR Data. ^{1}H NMR ($CDCl_3$, 400 MHz): δ 1.34 (d, J = 6.8 Hz, 3H, β-CH_3 Ala), 1.43 (s, 9H, C($CH_3)_3$), 2.75−2.77 (m, 1H, β-CH_2 Cys), 2.84−2.89 (m, 1H, β-CH_2 Cys), 3.15−3.20 (m, 1H, β-CH_2 BOT), 3.24−3.29 (m, 1H, β-CH_2 BOT), 3.70−3.72 (d, J = 5.6 Hz, 2H, CH_2 Bzl), 3.73 (s, 3H, OCH_3), 4.24−4.27 (m, 1H, α-H Cys), 4.42−4.47 (m, 1H, α-H Ala), 4.84−4.88 (m, 1H, α-H BOT), 5.41 (d, J = 7.2 Hz, 1H, NH Cys), 6.84−6.89 (m, 2H, NH Ala and NH BOT), 7.11−7.13 (dd, J = 1.6 and 8.4 Hz, 1H, H6), 7.19−7.22 (m, 1H, H4′), 7.27−7.31 (m, 5H, 5 × Ph−*H*), 7.46 (d, J = 8.4 Hz, 1H, H7), 7.48 (d, J = 1.6 Hz, 1H, H4), 7.59 (dd, J = 1.2, 5.2 Hz, 1H, H5′), 7.97−7.98 (br d, J = 2.8 Hz, 1H, H3′).

^{13}C NMR ($CDCl_3$, 100 MHz): δ 17.74 (β-CH_3 Ala), 28.24 (C($\underline{C}H_3)_3$), 33.66 (β-CH_2 Cys), 36.51 (CH_2 Bzl), 37.70 (β-CH_2 BOT), 49.10 (α-C Ala), 52.47 (OCH_3), 53.53 (α-C Cys), 53.65 (α-C BOT), 80.38 ($\underline{C}(CH_3)_3$), 110.49 (C7), 119.89 (C4), 126.66 (C6), 127.20 (C 4″), 128.60 (C4′), 128.94 (C2″ and C6″), 130.80 (C3′), 131.01 (C5′), 133.10 (C5), 137.91 (C1″), 141.18 (C3a), 149.39 (C7a), 155.35 (C═O Boc), 159.38 (C2 and C2′), 170.60 (C═O Cys), 171.35 (C═O Ala and C═O BOT).

IR (NaCl windows, cm^{-1}): ν(NH st) 3300, ν(C═O aliphatic ester) 1751, ν(COO^-) 1734, ν(C═O st) 1695, ν(O−C═N, C═N derivatives) 1690, ν(C═C benzene) 1669, ν($-CH_2$ δ) 1457, ν($-CH_3$ δ) 1366, ν(thiophene) 3100 (CH st), 1534 (CH γ).

MALDI-TOF-MS [calcd (found)]: [**4**H]$^+$, 667.8 (667.5), 10%; [**4**-BocH]$^+$, 567.8 (567.5), 55%; [$C_{15}H_{14}N_2O_3SH$]$^+$, 303.0 (303.5), 100%

*4. Synthesis of Boc-BOT-Cys(Bzl)-Trp(ZNO$_2$)-OMe (**7**).* **3** (0.07 g, 1.25×10^{-4} mol) was dissolved in distilled DMF (2 mL) cooled in an ice bath before the addition of HOBt (0.02 g, 1.48×10^{-4} mol) and DCC (0.03 g, 1.45×10^{-4} mol) and then stirred for 30 min, maintaining the temperature at 0 °C. NH_2-Trp(ZNO_2)-OMe (0.05 g, 1.26×10^{-4} mol) was then added, and the solution was stirred for 1 h in an ice bath and 1 h at room temperature. The solvent was evaporated under reduced pressure, and the residue was treated with cooled acetone to remove DCU through filtration. The solvent was evaporated, and the residue was purified by column chromatography with silica gel (1:1 ethyl acetate/hexane, followed by 200:1 ethyl acetate/MeOH). The fractions were combined, and the final product **7** was recrystallized from methanol: white solid (0.49 g, 51%), mp 198−200 °C, $C_{49}H_{48}N_6O_{11}S_2$, fw = 961.07. Elem anal. Calcd: C, 61.2; H, 5.0; N, 8.7; S, 6.7. Found: C, 61.4; H, 5.2; N, 8.4; S, 6.7.

NMR Data. ^{1}H NMR (DMSO-d_6, 400 MHz): δ 1.21 (s, 9H, C(CH_3)$_3$), 2.55−2.60 (m, 1H, β-CH_2 Cys), 2.66−2.78 (m, 2H, β-CH_2 Cys and β-CH_2 BOT), 2.98−3.03 (m, 1H, β-CH_2 BOT), 3.10−3.21 (m, 2H, β-CH_2 Trp), 3.57 (s, 3H, OCH_3), 3.74 (s, 2H, CH_2 Bzl), 4.18−4.24 (m, 1H, α-H Cys), 4.57−4.67 (m, 2H, α-H BOT and α-H Trp), 5.48 (s, 2H, CH_2 ZNO_2), 6.89 (d, J = 8.8 Hz, 1H, NH BOT), 7.20−7.33 (m, 10H, 5 × Ph−*H* Bzl, H2′, and H6′ ZNO_2, H6 BOT, H2 and H5 Trp), 7.54−7.61 (m, 3H, H4 and H7 BOT, H4 Trp), 7.67−7.73 (m, 3H, H6 Trp, H7 Trp, and H4′BOT), 7.89 (dd, J = 1.2 and 3.6 Hz, 1H, H3′ZNO_2), 7.92 (dd, J = 1.2 and 4.8 Hz, 1H, H5′ZNO_2), 8.03 (d, J = 8.4 Hz, 1H, NHCys), 8.21 (d, J = 8.8 Hz, 2H, H3′ and H5′ BOT), 8.69 (d, J = 7.2 Hz, NH Trp).

^{13}C NMR (DMSO-d_6, 100 MHz): δ 26.31 (β-CH_2 BOT), 27.99 (C($\underline{C}H_3$)$_3$), 33.07 (β-CH_2 Cys), 35.25 (β-CH_2 BOT), 37.35 (CH_2 Bzl), 51.99 (OCH_3), 52.15 (α-C BOT and α-C Trp), 55.95 (α-C Cys), 66.68 (CH_2 ZNO_2), 78.06 ($\underline{C}(CH_3)_3$, 109.90 (C7 BOT), 114.67 (C3 Trp), 116.71 (C7 Trp), 119.13 (C4 Trp), 120.5 (C4 BOT), 123.03 (C5 Trp), 123.62 (C3′ ZNO_2), 123.88 (C6 Trp), 124.71 (C2 Trp), 126.72 (C6 BOT), 126.77 (C 4″), 128.27 (C3″ and C5″), 128.56 (C4′), 128.64 (C2″ and C6″), 128.83 (C2), 128.94 (C2′ ZNO_2), 130.04 (C3a Trp), 130.31 (C3′), 131.76 (C5′), 134.77 (C5 BOT), 135.13 (C7a Trp), 138.33 (C1″), 141.28 (C3a BOT), 142.97 (C1′ ZNO_2), 147.23 (C4′ ZNO_2), 148.61 (C7a BOT), 155.17 (C═O Boc), 158.35 (C2′), 170.26 (C═O Cys), 171.41 (C═O Trp and C═O BOT).

IR (NaCl windows, cm^{-1}): ν(NH st) 3311, ν(NH st tryptophan) 3054, 2984, ν(COO$^-$ st) 1738, ν(C═O) 1687, ν(C═C benzene) 1634, ν(−CH_2 δ) 1450, ν(−CH_3 δ) 1392, 1367, ν(thiophene) 3054 (CH st), 1525 (CH γ), 1422, 1433, 739 (CH δ_{oop}).

MALDI-TOF-MS [calcd (found)]: [**7**Na]$^+$, 984.0 (983.6), 20%; [**7**-BocNa]$^+$, 884.0 (884.5), 15%; [$C_{34}H_{33}N_5O_3S_2H$]$^+$, 625 (625.8), 98%; [$C_{35}H_{33}N_5O_5S_2H$]$^+$, 669 (669.8), 85%; [$C_{11}H_7NOSH\cdot CH_3CN$]$^+$, 243.2 (243.5), 100%.

*5. Synthesis of H-BOTT-OMe (**8**).* Compound **8** was obtained by the removal of the Boc group from compound Boc-BOTT-OCH_3, whose preparation was already published.[17] Compound Boc-BOTT-OCH_3 was dissolved in 1 mL of dichloromethane and 1 mL of TFA and stirred for 2 h. The solution was evaporated under reduced pressure, yielding a green salt. It was dissolved in an aqueous solution (pH = 8) and extracted with ethyl acetate (3 × 5 mL). After drying with anhydrous magnesium sulfate, compound **8** was isolated as a yellow solid (0.06 g, 90%) by evaporation: $C_{19}H_{16}N_2O_3S_2$, fw = 384.1. Elem anal. Calcd: C, 59.4; H, 4.2; N, 7.3; S, 16.7. Found: C, 59.5; H, 4.5; N, 7.4; S, 16.6.

NMR Data. ^{1}H NMR (DMSO, 400 MHz): δ 3.06−3.15 (m, 2H, β-CH_2 BOTT), 3.49 (s, 2H, NH_2), 3.70 (s, 3H, OCH_3), 4.32−4.36 (m, 1H, α-H BOTT), 7.16−7.18 (m, 1H, H4″), 7.23 (d, J = 3.6 Hz, 1H, H4′), 7.49−7.60 (m, 3H, H3″, H5″, H6), 7.70 (d, J = 8.4 Hz, 1H, H7), 7.80 (d, J = 1.6 Hz, 1H, H4), 7.90 (d, J = 4.0 Hz, 1H, H3′).

^{13}C NMR ($CDCl_3$, 100 MHz): δ 38.81 (β-CH_2 BOTT), 52.60 (OCH_3), 57.8 (α-C BOTT), 110.64 (C7), 120.26 (C4), 125.21 (C4′), 125.89 (C5″), 125.96 (C3″), 126.18 (C6), 126.84 (C2′), 127.35 (C4″), 128.67 (C3′), 131.68 (C5), 135.00 (C2″), 141.63 (C5′), 141.69 (C3a), 149.26 (C7a), 158.13 (C2).

IR (NaCl windows, cm^{-1}): ν(C═O aliphatic ester) 1751, ν(COO−) 1734, ν(C═O st) 1695, ν(O−C═N, C═N derivatives) 1690, ν(C═C benzene) 1669, ν(−CH_2 δ) 1457, ν(−CH_3 δ) 1366, ν(thiophene) 3100 (CH st), 1534 (CH γ).

ESI-MS [calcd (found)]: [**8**]H$^+$, 385.06 (385.06), 100%.

*6. Synthesis of Boc-BOTT-Cys(Bzl)-OMe (**9**).* Boc-BOTT-OH (0.11 g, 2.41×10^{-4} mol) was dissolved in freshly distilled DMF (2 mL) cooled in an ice bath, and then HOBt (0.03 g, 2.41×10^{-4} mol) and DCC (0.05 g, 2.41×10^{-4} mol) were added. The mixture was stirred in an ice bath for 30 min.

In a separated flask, HCl·H-Cys(Bzl)-OMe (0.06 g, 2.41×10^{-4} mol) was neutralized with triethylamine (32 μL, 2.41×10^{-4} mol) in freshly distilled DMF with stirring for 30 min. The mixture was filtered and added to the solution containing Boc-BOTT-OH. The solution was stirred for 1 h in an ice bath and another 1 h at room temperature. The solvent was then evaporated under reduced pressure, and the residue was treated with cooled acetone to remove DCU through filtration. The acetone was evaporated, and the residue was purified by column chromatography with silica gel (eluent: 2:3 ethyl acetate/hexane). The fractions were combined, and the product was obtained as a yellow solid (0.13 g, 70%): mp 181−183 °C, $C_{34}H_{35}N_3O_6S_3$, fw = 677.8. Elem anal. Calcd: C, 60.2; H, 5.2; N, 6.2; S, 14.2. Found: C, 60.3; H, 5.2; N, 6.1; S, 14.0.

NMR Data. ^{1}H NMR ($CDCl_3$, 400 MHz): δ 1.42 (s, 9H, C(CH_3)$_3$), 2.78−2.89 (m, 2H, β-CH_2 Cys), 3.20 (d, J = 6.4 Hz, 2H, β-CH_2 BOTT), 3.66 (s, 2H, CH_2 Bzl), 3.70 (s, 3H, OCH_3), 4.41−4.43 (m, 1H, α-H BOTT), 4.73−4.77 (m, 1H, α-H Cys), 4.99−5.02 (br s, 1H, NH Cys), 6.61 (d, J = 7.2 Hz, 1H, NH BOTT), 7.07−7.09 (m, 1H, H4″), 7.20−7.33 (m, 8H, 5 × Ph−*H*, H3″, H5″, H6), 7.23 (d, J = 3.6 Hz, 1H, H4′), 7.44 (d, J = 8.4 Hz, 1H, H7), 7.54 (d, J = 1.6 Hz, 1H, H4), 7.79 (d, J = 4.0 Hz, 1H, H3′).

^{13}C NMR ($CDCl_3$, 100 MHz): δ 28.24 (C($\underline{C}H_3$)$_3$), 33.37 (β-CH_2 Cys), 36.55 (CH_2 Bzl), 38.22 (β-CH_2 BOTT), 51.67 (α-C Cys), 52.61 (OCH_3), 55.85 (α-C BOTT), 80.37 ($\underline{C}(CH_3)_3$), 110.39 (C7), 120.36 (C4), 125.47 (C4′), 125.10 (C5″), 125.93 (C3″), 126.38 (C6), 127.23 (C4‴), 127.45 (C2′), 128.17 (C4″), 128.56 (C3‴ and C5‴), 128.89 (C2‴ and C6‴), 130.68 (C3′), 133.25 (C5), 136.24 (C2″), 137.60 (C1‴), 142.33 (C5′), 142.47 (C3a), 149.64 (C7a), 155.23 (C═O Boc), 159.02 (C2), 170.66 (C═O Cys), 170.88 (C═O BOTT).

IR (NaCl windows, cm^{-1}): ν(NH st) 3300, ν(OH) 3423; ν(COO$^-$ st) 1731, ν(C═O) 1696, ν(C═C benzene) 1663; ν(−CH_2 δ) 1453, ν(−CH_3 δ) 1369, ν(thiophene) 3061 (CH st), 1534 (CH γ), 746 (CH δ_{oop}).

MALDI-TOF-MS [calcd (found)]: [**9**Na]$^+$, 700.1 (700.03), 10%; [**9**-BocNa]$^+$, 599.2 (599.9), 45%.

*7. Synthesis of Boc-Cys(Bzl)-Ala-BOTT-OMe (**10**).* **6** (0.12 g, 3.14×10^{-4} mol) was dissolved in freshly distilled DMF (2 mL) cooled in an ice bath, and then HOBt (0.045 g, 3.33×10^{-4} mol) and DCC (0.064 g, 3.10×10^{-4} mol) were added. The mixture was then stirred in an ice bath for 30 min before compound **8** (0.11 g, 2.99×10^{-4} mol) was added, and the final mixture was stirred for 1 h in an ice bath and 1 h at room temperature. The solvent was evaporated under reduced pressure, and the residue was treated with cooled acetone to remove DCU through filtration. The solvent was evaporated, and the residue was purified by column chromatography with silica gel (eluent: 1:1 ethyl acetate/hexane). The fractions were combined, and the product was recrystallized from methanol to obtain a yellow solid (0.06 g, 26%): mp 162−166 °C, $C_{37}H_{40}N_4O_7S_3$, fw = 748.9. Elem anal. Calcd: C, 59.3; H, 5.4; N, 7.5; S, 12.8. Found: C, 59.5; H, 5.5; N, 7.2; S, 12.9.

Scheme 2. Fragments of the Ligands obtained in MALDI-TOF-MS

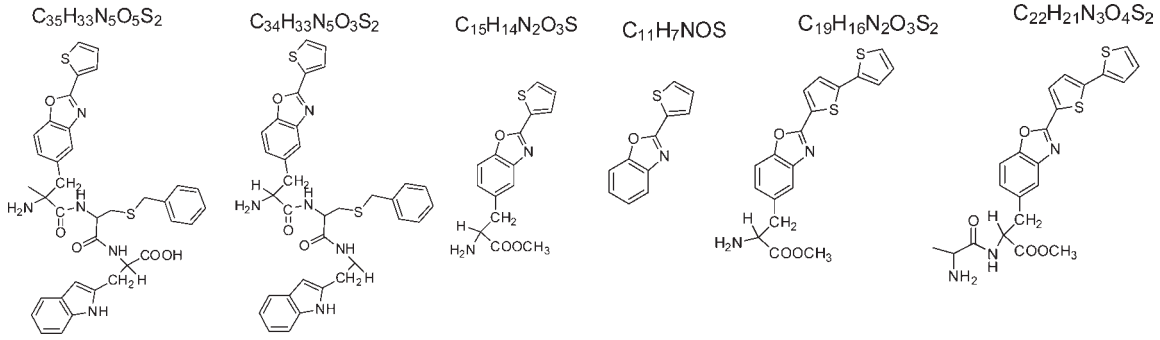

NMR Data. ^{1}H NMR (DMSO-d_6, 300 MHz): δ 1.16−1.18 (d, J = 6.9 Hz, 3H, β-CH_3 Ala), 1.37 (s, 9H, $C(CH_3)_3$), 2.43−2.48 (m, 1H, β-CH_2 Cys), 2.65−2.71 (m, 1H, β-CH_2 Cys), 2.99−3.07 (m, 1H, β-CH_2 BOTT), 3.12−3.20 (m, 1H, β-CH_2 BOTT), 3.59 (s, 3H, OCH_3), 3.69 (s, 2H, CH_2 Bzl), 4.11−4.19 (m, 1H, α-H Cys), 4.24−4.33 (m, 1H, α-H Ala), 4.49−4.56 (m, 1H, α-H BOTT), 6.97 (d, J = 8.4 Hz, 1H, NH Ala), 7.14−7.24 (m, 6H, 5 × Ph−*H* and H4″), 7.46 (d, J = 3.9 Hz, 1H, H4′), 7.52 (dd, J = 1.2 and 3.9 Hz, 1H, H3″), 7.58 (d, J = 1.2 Hz, 1H, H4), 7.62 (d, J = 8.7 Hz, 1H, H7), 7.65 (dd, J = 1.2 and 6.0 Hz, 1H, H5″), 7.87 (d, J = 3.9 Hz, 1H, H3′), 7.99 (d, J = 7.2 Hz, 1H, NH Cys), 8.33 (d, J = 7.5 Hz, 1H, NH BOTT).

^{13}C NMR (DMSO-d_6, 75.4 MHz): δ 18.34 (β-CH_3 Ala), 28.15 ($C(\underline{C}H_3)_3$), 33.54 (β-CH_2 Cys), 35.21 (CH_2 Bzl), 36.42 (β-CH_2 BOTT), 47.91 (α-C Ala), 51.92 (OCH_3), 53.63 (α-C Cys), 53.80 (α-C BOTT), 78.28 ($\underline{C}(CH_3)_3$), 110.26 (C7), 119.85 (C4), 125.25 (C4′), 125.97 (C3″), 126.48 (C2′), 126.72 (C4‴), 126.76 (C6), 127.36 (C5″), 128.28 (C3‴ and C5‴), 128.75 (C4″), 128.86 (C2‴ and C6‴), 131.48 (C3′), 134.16 (C5), 135.15 (C2″), 138.35 (C1‴), 141.50 (C5′), 141.54 (C3a), 148.89 (C7a), 155.27 (C=O Boc), 158.02 (C2), 170.11 (C=O Cys), 171.61 (C=O BOTT), 172.06 (C=O Ala).

IR (NaCl windows, cm^{-1}): ν(NH st) 3300, ν(C=O aliphatic ester) 1751, ν(COO−) 1734, ν(C=O st) 1695, ν(O−C=N, C=N derivatives) 1690, ν(C=C benzene) 1669, ν(−CH_2 δ) 1457, ν(−CH_3 δ) 1366, ν(thiophene) 3100 (CH st), 1534 (CH γ).

MALDI-TOF-MS [calcd (found)]: [**10**-BocH]$^+$, 649.1 (649.5), 20%; [**10**-Boc-BznH]$^{+\cdot}$MeOH, 633.2 (633.4), 25%; $[C_{22}H_{21}N_3O_4S_2H]^+$, 456.1 (456.5), 35%; $[C_{19}H_{16}N_2O_3S_2H]^+$, 385.1 (385.5), 100% (see MALDI-TOF-MS fragments in Scheme 2).

Synthesis of AuNPs. Compound **1** (0.008 g, 2.62 × 10^{-5} mol) was dissolved in dry dichloromethane, DSP (0.011 g, 2.72 × 10^{-5} mol) was added, and the solution was stirred at room temperature overnight. The mixture was washed with water (3 × 3 mL), and the organic phase was dried with sodium sulfate and filtered. The filtered solution was evaporated and dried under reduced pressure to yield a pale-yellow solid.

The synthesis of AuNPs has been performed following the well-established and very efficient procedure proposed by Professors M. Brust and D. J. Schiffrin.[20]

$HAuCl_4$ (0.0876 mmol) was dissolved in 10 mL of water, while 0.41 mmol of TOAB (98%) was dissolved in 10 mL of CH_2Cl_2. A total of 1 mL of the gold-yellow aqueous solution was added to 1 mL of a CH_2Cl_2 solution of TOAB. The mixture was stirred until the complete phase transfer of the gold ions, which was clearly indicated by the total discoloration of the water phase and the contemporary turning of the organic one into a deep-ruby-red color. The organic phase was separated, and 0.005 mmol of the thyolate precursor was then added. To this vigorously stirring solution was added dropwise 1 mL of water containing 1.1 mmol of $NaBH_4$, and the color started to turn immediately from red to a very dark purple, typical of the formation of these metal nanoparticles. The solution was washed three times with water, and then the nanoparticles were isolated by precipitation with methanol followed by centrifugation. DLS: 4.2 ± 2.1 nm. TEM: 3 ± 2 nm.

Compound **4** (0.010 g, 1.53 × 10^{-5} mol) was stirred in mixed solvent TFA/dichloromethane (1:1, 1 mL) at room temperature for 2 h. The solvent was evaporated and the oily residue was dissolved in dichloromethane; triethylamine was then added. After washing three times with water, the solution was evaporated under reduced pressure, yielding a solid residue. This solid (0.013 mmol) was dissolved in 2 mL of dried dichloromethane, DSP (0.013 mmol) was added, and the solution was stirred at room temperature overnight. The mixture was then washed with water (3 × 3 mL), dried with sodium sulfate, filtered, and finally evaporated under reduced pressure to yield a solid compound.

The AuNPs were then prepared following the procedure described above but adding 0.005 mmol of the thyolated **4** instead of **1** before gold reduction. DLS: 15.1 ± 3.6 nm. TEM: 3.5 ± 2.5 nm.

Synthesis of Silica Nanoparticles Decorated with Compounds 8−10. Compound **8** (0.01 mmol) was dissolved in 1 mL of dichloromethane under stirring, triethylamine (0.02 mmol) and the linker 3-isocyanotopropylsilane (0.02 mmol) were then added, and the mixture was kept under stirring for 2 days. Substitution of the amino group by the silane derivative was evidenced by Silica-TLC (eluent: ethyl acetate). The dichloromethane was evaporated under reduced pressure to yield a yellow powder.

This solid was then dissolved in a mixture of 0.5 mL of ethanol, 0.5 mL water, 0.5 mL of CH_3COOH, and 0.680 mL of a water solution of commercial Ludox AS-30 by Sigma-Aldrich (with a diameter of 15 ± 3 nm measured by TEM and a hydrodynamic diameter of 20 ± 3 nm obtained by DLS). This mixture was stirred at 80 °C for 2 days, and then 200 μL was withdrawn, dissolved in 1 mL of dichloromethane, and centrifuged at 8600 rpm, at 21 °C, for 10 min. The pellet was washed three times with methanol (3 × 1 mL) and finally dissolved in 0.5 mL of absolute ethanol.

Silica nanoparticles decorated with compounds **9** and **10** were also prepared following exactly the same procedure as that described above, after their deprotection and derivatization with 3-isocyanotopropylsilane, as in the case of **8**.

Photophysical Measurements. Absorption spectra were recorded on Perkin-Elmer Lambda 45 and Jasco 650 spectrophotometers and fluorescence spectra on a Perkin-Elmer LS55 spectrophotometer. The linearity of the fluorescence emission versus concentration was checked in the range used (10^{-4}−10^{-6} M). A correction for the absorbed light was performed when necessary.[21] The spectrophotometric characterizations and titrations were performed as follows: stock solutions of the ligands (ca. 10^{-3} M) were prepared by dissolving an appropriate amount of the compound in a 10 mL volumetric flask and diluting to the mark with absolute ethanol. A suitable dilution of these stock solutions down to 10^{-5}−10^{-6} M allowed one to titrate the ligands

dx.doi.org/10.1021/ic200792t |*Inorg. Chem.* 2011, 50, 8834–8849

2−**4** and **7**−**10** with increasing amounts (microliters) of standard solutions of the ions in absolute ethanol. All of the measurements were performed at 298 K. When indicated in the text, the absorption and fluorescence spectra were also performed for microsamples using a NanoDrop ND-1000 spectrophotometer and ND-3300 spectrofluorimeter. Also in this case, the linearity of the fluorescence emission versus concentration was checked for the range used (10^{-4}−10^{-6} M).

Luminescence quantum yields were measured using a solution of quinine sulfate in sulfuric acid (0.5M) as a standard ($[\phi] = 0.54$)[22] and were corrected for the different refraction indexes of the solvents.

Luminescence lifetime measurements were carried out by using a time-correlated single-photon-counting apparatus by Edinburg Instruments, as previously described.[23]

Detection Limit (LOD) Calculations. LOD is known as the smallest amount of analyte that can be measured "significantly different" from the blank.[24] We have measured the signal from n blank samples containing no analyte ($n = 6$) and calculated the mean value (y_{blank}). Then we have determined the standard deviation. LOD was obtained by the formula

$$y_{dl} = y_{blank} + 3std$$

where y_{dl} = signal detection limit and std = standard deviation.

MALDI-TOF-MS Measurements. The MALDI-MS spectra of soluble samples (1 or 2 $\mu g/\mu L$) such as metal salts were recorded using the conventional sample preparation method for MALDI-MS. A total of 1 μL of the solution containing 1 or 2 equiv of the metal was put on the sample holder on which the chelating ligand had been previously spotted. The sample holder was inserted in the ion source. A chemical reaction between the ligand and metal salts occurred in the holder, and complexed species were produced.

MALDI-TOF-MS analysis has been performed in a MALDI-TOF-MS model voyager DE-PRO biospectrometry workstation equipped with a nitrogen laser radiating at 337 nm from Applied Biosystems (Foster City, CA) at the REQUIMTE, Chemistry Department, Universidade Nova de Lisboa. The acceleration voltage was 2.0×10^4 kV with a delayed extraction time of 200 ns. The spectra represent accumulations of 5 × 100 laser shots. The reflection mode was used. The ion source and flight tube pressures were less than 1.80×10^{-7} and 5.60×10^{-8} Torr, respectively.

Physical Measurements. Elemental analyses were carried out on a Thermo Finnigan-CE Flash-EA 1112-CHNS by the REQUIMTE DQ, Universidade Nova de Lisboa Service, on a Fisons Instruments EA1108 microanalyzer at University of Vigo, or on a Leco CHNS 932 instrument at Center of Chemistry, University of Minho. IR spectra were recorded in NaCl windows using a Bio-Rad FTS 175-C spectrophotometer. NMR spectra were obtained on a Varian Unity Plus spectrometer at an operating frequency of 300 MHz for ^{1}H NMR and 75.4 MHz for ^{13}C NMR or on a Bruker Avance III 400 at an operating frequency of 400 MHz for ^{1}H NMR and 100.6 MHz for ^{13}C NMR, using the solvent peak as an internal reference at 25 °C. All chemical shifts are given in ppm using δ_H Me_4Si = 0 ppm as the reference, and J values are given in hertz. Assignments were made by a comparison of the chemical shifts, peak multiplicities, and J values and were supported by spin decoupling−double resonance and bidimensional heteronuclear HMBC and HMQC correlation techniques. Electrospray ionization time-of-flight mass spectrometry (ESI-TOF-MS) spectra were carried at the Mass Spectra Laboratory in Universidade de Vigo, CACTI, on a Bruker FT MS APEX-Qe 7T FTCIR-MS spectrometer.

Particles Size Distribution. The nanoparticle size distributions were measured using DLS, with a Malvern Nano ZS instrument and a 633 nm laser diode.

TEM Measurements. For TEM investigations, a Philips CM 100 transmission electron microscope operating at 80 kV was used. A drop of nanoparticle in a dichloromethane solution was transferred onto holey carbon foils supported on conventional copper microgrids.

Table 1. Optical Data for 2−4 and 7−10 in Dichloromethane and in Absolute Ethanol

	UV−vis		fluorescence		
	λ_{exc} (nm)	log ε	λ_{em} (nm)	t (ns)	ϕ
2	316[a]	4.29[a]	394[a]		0.26[a]
	316[b]	4.28[b]	384[b]	1.5[b]	0.44[b]
3	316[a]	4.29[a]	395[a]		0.29[a]
	316[b]	4.29[b]	384[b]	1.5[b]	0.46[b]
4	316[a]	4.64[a]	396[a]		0.31[a]
	316[b]	4.32[b]	384[b]	1.5[b]	0.71[b]
7	316[a]	4.49[a]	395[a]		0.08[a]
	316[b]	4.26[b]	384[b]	<0.6[b]	0.06[b]
8	366[a]	4.29[a]	440[a]		0.25[a]
	366[b]	4.28[b]	440[b]	1.5[b]	0.43[b]
9	366[a]	4.29[a]	440[a]		0.26[a]
	366[b]	4.28[b]	440[b]	1.5[b]	0.44[b]
10	366[a]	4.29[a]	440[a]		0.29[a]
	366[b]	4.29[b]	440[b]	1.5[b]	0.46[b]

[a] Dichloromethane solution. [b] Absolute ethanol solution.

RESULTS AND DISCUSSION

Synthesis of Peptides. Synthesis of peptides **2**, **4**, and **7** was carried out by standard DCC/HOBt amino acid coupling procedures, while peptide **3** was obtained from **2** by cleavage of the ester protecting group with basic hydrolysis at the terminal carboxylic acid. Tripeptide **4** was obtained by the coupling of **1**[17] with **6**, and tripeptide **7** was obtained by the coupling of **3** and NH_2-Trp(ZNO_2)-OMe (see Scheme 1).

Synthesis of the emissive alanine derivative **8** was carried out by removal of the *N*-*tert*-butyloxycarbonyl (Boc) protecting group from the ligand Boc-BOTT-OCH_3.[17] Dipeptide **9** was obtained by the reaction between Boc-BOTT-OH and H-Cys-(Bzl)-OMe. Tripeptide **10** was obtained by a standard DCC/HOBt coupling reaction between precursor **6** and **8**.

All compounds synthesized were obtained in a good-to-moderate yield: 75% (**2**), 71% (**3**), 42% (**4**), 51% (**7**), 90% (**8**), 70% (**9**), and 26% (**10**).

All compounds were characterized by elemental analysis, ^{1}H and ^{13}C NMR, IR spectroscopy, MALDI-TOF-MS, melting point (see the Experimental Section), and UV−vis absorption and fluorescence emission spectroscopy (see Table 1).

The MALDI-TOF-MS spectra showed peaks corresponding to $[\mathbf{2}H]^+$ at 596.5 nm, $[\mathbf{3}H]^+$ at 582.5 nm, and $[\mathbf{4}H]^+$ at 667.5 nm, confirming the integrity of the studied peptides. The ESI spectra for **8** showed the peak $[\mathbf{8}H]^+$, 385.06 (385.06) 100%. The MALDI-TOF-MS spectra for the bithienyl dipeptide **9** presented peaks for $[\mathbf{9}Na]^+$, 700.1 (700.03) 10%, and $[\mathbf{9}\text{-BocNa}]^+$, 599.2 (599.9) 45%, while the tripeptide **10** originated several peaks; among them, the ones corresponding to $[\mathbf{10}\text{-BocH}]^+$, 649.1 (649.5) 20%, and $[\mathbf{10}\text{-Boc-BznH}]^+ \cdot$MeOH, 633.2 (633.4) 25%, are the most interesting.

The IR spectra of compounds **2**−**4**, **7**, **9**, and **10** presented a band at 3300 cm^{-1} assignable to the amide NH, as well as a band at ca. 1750−1650 cm^{-1} related to the urethane, ester, amide, and

dx.doi.org/10.1021/ic200792t |*Inorg. Chem.* 2011, 50, 8834–8849

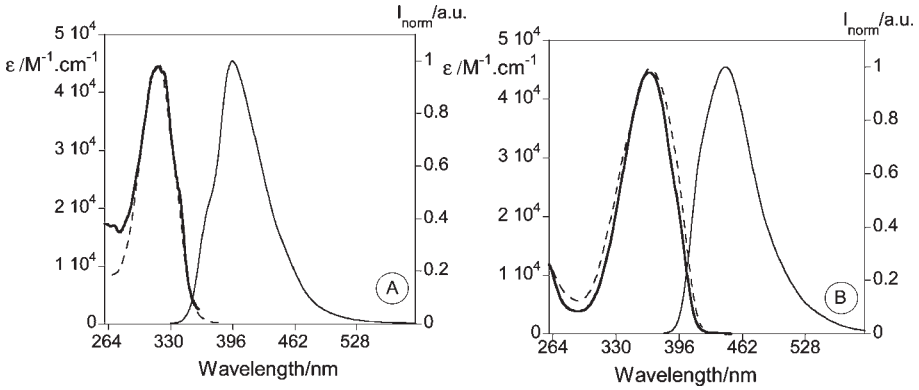

Figure 1. Room temperature absorption (bold line), normalized emission (full line, λ_{exc} = 316 nm in part A; λ_{exc} = 366 nm in part B), and excitation spectra (dotted line, λ_{em} = 396 nm in part A; λ_{em} = 440 nm in part B) of compounds **4** (A) and **10** (B) in dichloromethane.

carboxylic acid carbonyl groups. The ^{1}H NMR spectra of compounds **2**−**4**, **7**, **9**, and **10** presented the characteristic signals of the amino acid backbone NH and α-H and side-chain β-CH_3 (for Ala) or β-CH_2 (for BOT, BOTT, Cys, and Trp). The signals due to the heterocyclic ring present at the BOT, BOTT, and Trp side chains (thiophene, benzo[*d*]oxazole, and indole, respectively) were also visible. In the ^{13}C NMR spectra, the formation of the amide linkage was also confirmed by the appearance of the signal due to the amide carbonyl group at about 170−175 ppm.

Photophysical Studies. UV−vis absorption and emission spectra were recorded for all of the synthesized compounds, and their most significant photophysical data are gathered in Table 1. The absorption bands of **2**−**4** and **7** are all centered at 316 nm both in dichloromethane and in ethanol, while the emission bands present a maximum at around 395 nm in dichloromethane and 384 nm in ethanol. These bands can be attributed, in all cases, to the $\pi-\pi^*$ transition centered on the thienylbenzo[*d*]oxazole chromophore.[17] Compound **7** presents an additional absorption in the 250−300 nm region because of insertion of a tryptophan residue. The absorption and emission bands in dichloromethane and in absolute ethanol of the bithienylbenzo[*d*]oxazole derivatives **9** and **10** are centered at 366 and 440 nm, respectively. They are both remarkably red-shifted compared with the previous family of compounds, as expected because of their increased conjugation. As an example of the two classes of compounds, Figure 1 shows the absorption, emission, and excitation spectra in dichloromethane of **4** (part A) and **10** (part B).

The perfect match between the absorption and excitation spectra, moreover, rules out in all cases the presence of any emissive impurity. In the case of the tripeptide **7**, the coincidence between the absorption and excitation spectra indicates the occurrence of a very efficient energy transfer from the singlet excited state of the indole to the thienylbenzo[*d*]oxazole chromophore.

The fluorescence quantum yields of **2**−**4** and **8**−**10**, measured in dichloromethane and in absolute ethanol, are, in general, very high, with higher values in the latter solvent (Table 1). It has to be noted, however, that the addition of tryptophan to obtain the tripeptide **7** caused a strong decrease of the quantum yield. This quenching, accompanied by a parallel shortening of the excited-state lifetime, can be most probably attributed to an electron-transfer process because no energy-transfer process from the thienylbenzo[*d*]oxazole moiety is possible, with it being the lowest in energy.

Table 2. Complexation Constants for Peptides 2−4 and 7−10 in the Presence of Ag^+, Cu^{2+}, Ni^{2+}, and Hg^{2+} in Absolute Ethanol

peptides	metals	constants M:L
2	Hg^{2+}	1:1−8.97 ± 0.01
		2:1−13.42 ± 0.01
3	Ag^+	1:1−4.87 ± 0.01
		2:1−8.04 ± 0.05
	Cu^{2+}	1:1−7.45 ± 0.28
		2:1−13.99 ± 0.43
	Ni^{2+}	2:1−8.54 ± 0.03
	Fe^{3+}	1:2−11.95 ± 0.01
	Hg^{2+}	2:1−10.43 ± 0.01
4	Ag^+	1:1−4.74 ± 0.18
		2:1−8.88 ± 0.22
	Fe^{3+}	1:1−4.52 ± 0.01
	Hg^{2+}	2:1−11.81 ± 0.07
7	Hg^{2+}	1:1−7.06 ± 0.22
		2:1−12.47 ± 0.21
	Fe^{3+}	1:1−4.77 ± 0.01
9	Hg^{2+}	1:1−3.49 ± 0.18
		2:1−6.40 ± 0.06
10	Hg^{2+}	1:1−4.49 ± 0.21
		2:1−8.90 ± 0.08

As expected, the selective deprotection of the carboxylic group of the amino acid residue, which lies far apart from the chromophoric unit, on going from **2** to **3**, had only a minor influence on the fluorescence quantum yields.

Spectrophotometric and Spectrofluorimetric Titrations and Metal-Sensing Effects. The investigation of the sensing ability of compounds **2**−**4**, **7**, **9**, and **10** was carried out by UV−vis absorption and fluorescence emission studies in absolute ethanol solutions for Cu^{2+}, Ni^{2+}, Ag^+, Zn^{2+}, Cd^{2+}, Hg^{2+}, Pb^{2+}, and Fe^{3+}. The most significant data are gathered in Table 2.

Compound **2** showed spectral changes only upon the addition of Hg^{2+} that led to an emission quenching of ca. 88% with a relatively low association constant [Figure S1 in the Supporting Information; $\log\beta$ (M:L − 1:1) = 8.97 ± 0.01, and $\log\beta$ (M:L − 2:1) = 13.42 ± 0.01]. The minimum amount of Hg^{2+} detectable by **2** was estimated in ca. 1 ppm. A significantly different behavior was observed for compound **3**, presenting a carboxylic

dx.doi.org/10.1021/ic200792t |*Inorg. Chem.* 2011, 50, 8834–8849

complexing function instead of an ester. In this case, no changes were observed in the absorption spectra in the presence of metal ions, suggesting that the ground state of the peptide is not affected by complexation but instead induces strong changes in the excited state with a decrease of the fluorescence intensity of ca. 20%, 60%, and 100% upon the addition of Ag^+, Ni^{2+}, and Cu^{2+} (Figure 2), respectively. The fluorescence of compound **3** was also totally quenched in the presence of Fe^{3+} (see Figure S2A in the Supporting Information). All titration data were fitted using the global analysis program *SPECFIT*,[25] suggesting the formation of dinuclear complexes with molar ratio M:L, 2:1 for Ag^+, Ni^{2+}, and Cu^{2+}. In the case of Fe^{3+}, a different stoichimetry was obtained for the complex (M:L, 1:2), and this could suggest the formation of an adductlike species. However, without any X-ray crystal structure, one cannot infer too much with the metal-ion coordination binding modes. The minimum amounts detectable by **3** were 0.74 ppm (Ag^+), 2.04 ppm (Ni^{2+}), 0.11 ppm (Cu^{2+}), and 1.46 ppm (Fe^{3+}).

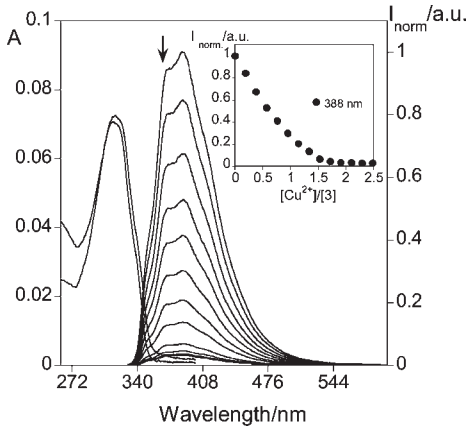

Figure 2. Absorption and emission spectra of **3** in the presence of increasing amounts of Cu^{2+} in an absolute ethanol solution. Inset: emission intensity at 388 nm as a function of $[Cu^{2+}]/[\mathbf{3}]$ (T = 298 K; $[\mathbf{3}] = 3.22 \times 10^{-6}$ M; λ_{exc} = 316 nm).

The spectral variations observed for these metal titrations, compared with the results previously published for ligand **1**,[17] support the hypothesis of a two-step complexation, with the first one involving the unprotected carboxylic group and the amine of the amino acid. The values of the association constants follow the trend $Cu^{2+} > Ni^{2+} > Ag^+$, which can be reasonably explained by taking into account that the more available donor atoms present in this dipeptide system are nitrogen and oxygen. On the other hand, Hg^{2+} gave an emission quenching of 75% (Figure S3 in the Supporting Information) with an association constant of log β (M:L − 2:1) = 10.43 ± 0.01. The minimum amount of Hg^{2+} detectable by **3** was 0.72 ppm.

In compound **4**, the insertion of an additional alanine unit between the chromophore and the cysteine leads to elongation of the spacer between the receptor and the signaling unit with interesting effects on the complexation ability and response of

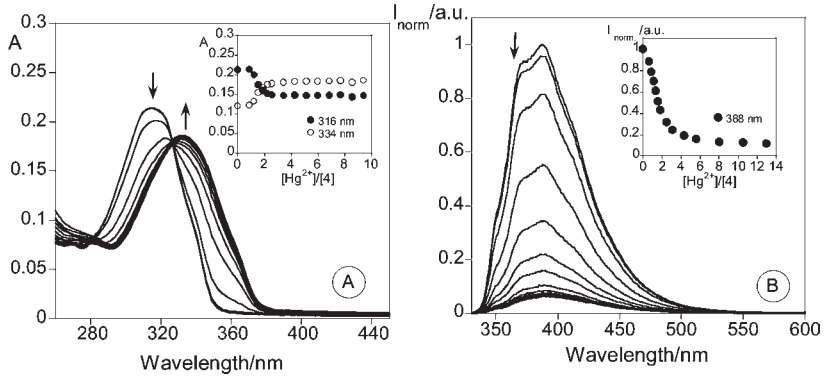

Figure 3. Spectrophotometric (A) and spectrofluorimetric (B) titrations of **4** with increasing amounts of Hg^{2+} in an absolute ethanol solution. Inset: absorption at 316 and 334 nm (A) and the emission intensity at 388 nm (B) as a function of $[Hg^{2+}]/[\mathbf{4}]$ (T = 298 K; $[\mathbf{4}] = 8.8 \times 10^{-6}$ M; λ_{exc} = 316 nm).

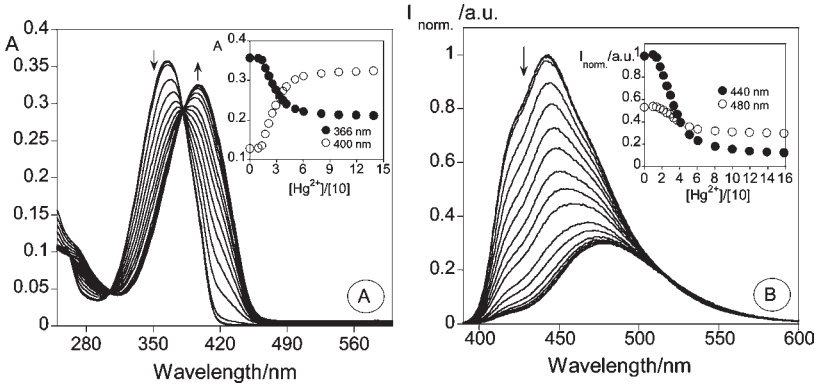

Figure 4. Spectrophotometric (A) and spectrofluorimetric (B) titrations of **10** with increasing amounts of Hg^{2+} in an absolute ethanol solution. Inset: absorption at 366 and 400 nm (A) and emission intensity at 440 and 480 nm (B) as a function of $[Hg^{2+}]/[\mathbf{10}]$ (T = 298 K; $[\mathbf{10}] = 7.69 \times 10^{-6}$ M; $[Hg(CF_3SO_3)_2] = 3.76 \times 10^{-3}$ M; λ_{exc} = 366 nm).

dx.doi.org/10.1021/ic200792t |*Inorg. Chem.* 2011, 50, 8834–8849

Table 3. MALDI-TOF-MS Peaks of Free Compounds 2−4 and 7−10

peptides	species	MALDI-TOF-MS calcd (found), %
2	$[\mathbf{2}H]^+$	596.7 (596.5), 25%
	$[\mathbf{2}H\cdot 5H_2O]^+$	686.7 (686.4), 68%
	$[\mathbf{2}\text{-BocH}]^+$	496.6 (496.4), 40%
	$[C_{11}H_7NOSNa]^+$	225 (225.6), 100%
3	$[\mathbf{3}H]^+$	582.7 (582.5), 25%
	$[\mathbf{3}\text{-BocH}]^+$	482.6 (482.5), 5%
	$[C_{11}H_7NOSNa]^+$	225 (225.6), 100%
4	$[\mathbf{4}H]^+$	667.8 (667.5), 10%
	$[\mathbf{4}\text{-BocH}]^+$	567.8 (567.5), 55%
	$[C_{15}H_{14}N_2O_3SH]^+$	303 (303.5), 100%
7	$[\mathbf{7}Na]^+$	984 (983.6), 20%
	$[\mathbf{7}\text{-BocNa}]^+$	884 (884.5), 15%
	$[C_{34}H_{33}N_5O_3S_2H]^+$	625 (625.8), 98%
	$[C_{35}H_{33}N_5O_5S_2H]^+$	669 (669.8), 85%
	$[C_{11}H_7NOSH.CH_3CN]^+$	243.2 (243.5), 100%
8	$[\mathbf{8}H]^+$	385.06 (385.06), 100%
9	$[\mathbf{9}Na]^+$	700.1 (700.03), 10%
	$[\mathbf{9}\text{-BocNa}]^+$	599.2 (599.9), 45%
10	$[\mathbf{10}\text{-BocH}]^+$	649.1 (649.5), 20%
	$[\mathbf{10}\text{-Boc-BznH-MeOH}]^+$	633.2 (633.4), 25%
	$[C_{22}H_{21}N_3O_4S_2H]^+$	456.1 (456.5), 35%
	$[C_{19}H_{16}N_2O_3S_2H]^+$	385.1 (385.5), 100%

this compound. Figure 3 shows the changes in the absorption (A) and emission (B) spectra of **4** upon the addition of increasing amounts of Hg^{2+}.

In particular, the addition of the first equivalent of Hg^{2+} did not induce any change in the spectrum of **4**, while the addition of the second equivalent caused a significant absorption change, with an isosbestic point at 328 nm and an emission quenching of 95%. This suggests that the complexation of the first metal ion can probably involve the peptide far from the chromophore, while the second metal equivalent can be complexed by the donor atoms present on the chromophore.[17] The minimum quantities of metal ions detectable by **4** in absolute ethanol were 1.85 ppm (Ag^+) and 0.71 ppm (Hg^{2+}).

All of the results discussed so far show that the insertion of alanine moieties on going from **2** to **4** leads to a higher affinity toward Hg^{2+} ions, and this is of particular interest for the design of more and more efficient chemosensors.

Among the other cations studied, the presence of Ag^+ induced some changes in the photophysical properties of **4**, namely, a red shift in the absorption spectra of 6 nm (from 316 to 322 nm) and a 65% quenching of the emission intensity (data not shown), but with smaller association constants. Also, the addition of increasing amounts of Fe^{3+} to this ligand in an ethanol solution induced significant changes in the photophysical properties and, in particular, an almost complete quenching of its emission intensity (Figure S2B in the Supporting Information). On the other side, the fitting of these data revealed a 1:1 stoichiometry of the complex but an association constant of several orders of magnitude lower than the one with mercury.

With the aim of introducing an additional chromophore in the peptide skeleton to enrich the photophysical properties, an emissive tryptophan unit was added to **3**, yielding the tripeptide

Table 4. MALDI-TOF-MS Most Important Peaks of Compounds 2 and 4 in the Presence of 1 or 2 equiv of Ag^+, Cu^{2+}, and Hg^{2+}

peptides	metal	species	MALDI-TOF-MS calcd (found), %
2	Ag^+	$[\mathbf{2}Ag]^+$	702.7 (702.6), 53%
		$[\mathbf{2}\cdot 2AgBF_4]^+$	897.3 (897.5), 15%
	Cu^{2+}	$[\mathbf{2}\cdot 2Cu\cdot 3CF_3SO_3Na]^+$	589.5 (589.4), 30%
	Hg^{2+}	$[\mathbf{2}H_2Hg(CF_3SO_3)_4Na]^+$	809 (809.6), 15%
4	Ag^+	$[\mathbf{4}Ag]^+$	775 (775.5), 35%
		$[\mathbf{4}\text{-Boc}\cdot Ag]^+$	675 (675.4), 60%
	Cu^{2+}	$[\mathbf{4}H_2Cu\cdot 3CF_3SO_3H_2O]^+$	629.5 (629.5), 100%
		$[\mathbf{4}\cdot 2Cu\cdot 3CF_3SO_3Na]^+$	631.9 (631.5), 80%
		$[\mathbf{4}H_2Cu_4CF_3SO_3\cdot CH_3CH_2OH\cdot Na]^+$	730 (729.6), 55%
	Hg^{2+}	$[\mathbf{4}HHg(CF_3SO_3)_2H_2O\cdot Na]^+$	538.5 (538.5), 50%

7. In this case, the absorption spectra after the addition of increasing amounts of Hg^{2+} did not show any change, while the fluorescence intensity was again strongly quenched (by ca. 80%; Figure S4 in the Supporting Information). It has to be noted that the estimated association constant (see Table 2) with Hg^{2+} for **7** is the highest observed among all of the peptides reported here for this metal ion. Interestingly, a relative enhancement of the fluorescence of 14% for Ag^+ and of 23% for Zn^{2+} and a quenching of 100% for Fe^{3+} were also observed, but with smaller association constants. Moreover, no changes were recorded for other metal ions (Cu^{2+}, Ni^{2+}, Cd^{2+}, and Pb^{2+}). The minimum quantity of Hg^{2+} observed was 3.12 ppm.

Compound **9**, a dipeptide containing the bithienylbenzo-[*d*]oxazole chromophore, showed changes upon the addition of various metal ions, namely, Cu^{2+}, Zn^{2+}, Ag^+, Fe^{3+}, and Hg^{2+}, only in the emission spectra. In particular, the addition of 1 equiv of Fe^{3+}, Cu^{2+}, or Hg^{2+} induced a quenching of the fluorescence emission of ca. 20%. On the other hand, the addition of increasing amounts of Zn^{2+} or Ag^+ to **9** induced a small emission increase of ca. 12% and 14%, respectively. The minimum quantity of Hg^{2+} detectable was estimated to be ca. 3 ppm.

As was already observed for the series **2**−**4**, insertion of an alanine moiety into the backbone of **9** to give **10** changed dramatically its response to the presence of transition-metal ions. In particular, the addition of Ag^+ ions (Figure S5 in the Supporting Information) induced a very small decrease and a red shift ($\Delta\lambda$ = 11 nm) of the band centered at 366 nm in the absorption spectra and an increase of 45% of the intensity of the emission, which was also red-shifted ($\Delta\lambda$ = 15 nm). On the other hand, the addition of Fe^{3+} led to a significant but not complete quenching of the fluorescence emission (Figure S2C in the Supporting Information).

As can be seen from Figure 4, the addition of Hg^{2+} induced even more pronounced effects. In particular, as was already observed for **4**, the first equiv of Hg^{2+} did not cause any spectral change, while the second equiv led to a decrease in the absorbance in the range of 366−383 nm and an increase at higher wavelengths, with an isosbestic point at λ = 383 nm. The color of the solution changed consequently from colorless to yellow. The strong quenching (92%) of the emission intensity was also accompanied by a large red shift of the band maximum from 440 to 480 nm. This result is of particular interest because it makes **10** a ratiometric chemosensor. The values of the

dx.doi.org/10.1021/ic200792t |*Inorg. Chem.* 2011, 50, 8834–8849

Scheme 3. Schematization of the Synthesis of AuNPs Decorated with 1

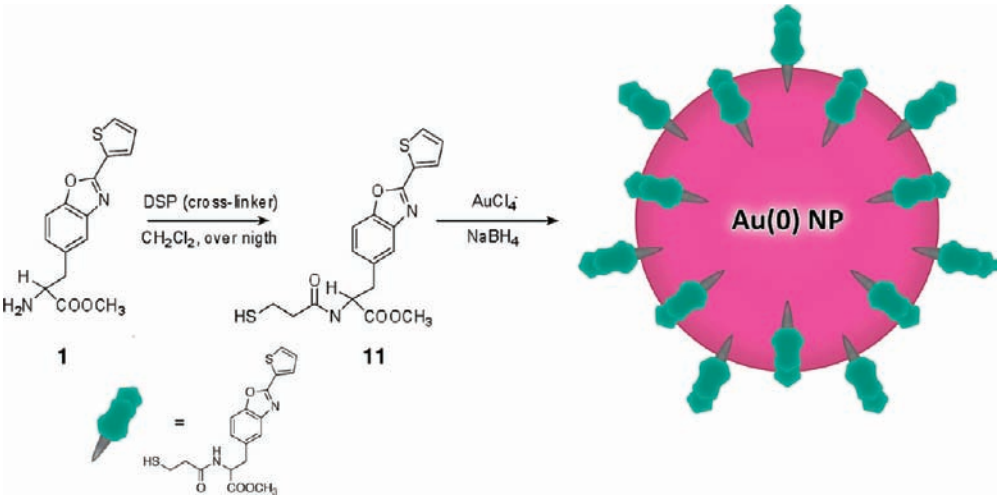

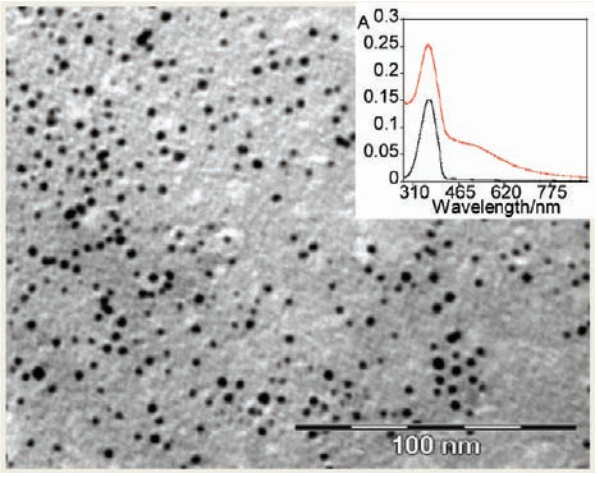

Figure 5. TEM picture of AuNPs functionalized with **1**. Inset: Absorption spectra in dichloromethane of **1** (black line) and of AuNPs (red line) decorated with **1** (T = 298 K; λ_{exc} = 316 nm).

association constants calculated for ligand **10** with Hg^{2+} ($\log \beta_{11}$ (M:L − 1:1) = 4.49 ± 0.21 and $\log \beta_{21}$ = 8.90 ± 0.08) indicate how the introduction of the second thiophene ring resulted in a significant affinity reduction toward these ions. Compound **10** was estimated to be able to detect down to ca. 1 ppm of Hg^{2+}.

To have a clearer picture of the intensity changes of the ligands versus the different metal ions added, we have reported a column graph (Figure S6 in the Supporting Information) of the normalized (with respect to the uncomplexed ligand) emission intensity for compounds **3**, **4**, **7**, and **10**. The most significant response changes were observed with Cu^{2+} in the case of **3** and with Hg^{2+} for compounds **4**, **7**, and **10**.

MALDI-TOF-MS Studies. In order to explore the possible applications of these new species as MALDI-TOF-MS active matrixes, peptides **2**−**4** and **7** were studied with this technique as such, in the absence of any other external organic matrix.

To perform the metal titrations, two different strategies were explored: a dried droplet solution and a layer-by-layer deposition sample preparation. In the first set of experiments, two solutions containing a ligand, and in particular **2** or **4** (1 μg/μL), and the metal salt (1 μL) were mixed and shaken before insertion in the MALDI-TOF-MS sample holder. The second method consisted of a layer-by-layer deposition of the different solutions: at first, a solution of peptide **2** or **4** was spotted in the MALDI-TOF-MS plate and then dried in vacuum; subsequently, 1 μL of the solution containing the metal salt was placed on the same sample holder and dried. Finally, the plate was inserted into the ion source. The most significant difference between the two procedures is that, in second case, the complexation reaction between the ligand and metal salts occurred directly in the holder, and the complex species were produced in the gas phase.

In general, the peaks corresponding to the protonated ligand and several fragments were perfectly observed (Table 3 and Scheme 2)

Compounds **2** and **4** were investigated as such and with 1 or 2 equiv of Ag^+, Cu^{2+}, or Hg^{2+} (Table 4), following both procedures for preparation of the sample. The formation of mononuclear and dinuclear complexes was evidenced by the appearance of several peaks clearly attributable to the metal complexes with these two stoichiometries. The most intense peaks were recorded upon the addition of Cu^{2+} or Hg^{2+}, confirming the affinity trends already observed in solution.

AuNPs. In order to study the effects of the peptide length in stabilizing AuNPs, compounds **1** and **4** were selected to be properly functionalized for the synthesis of decorated AuNPs. These compounds were therefore derivatized with a suitable cross-linker (DSP; Scheme 3) and then used as capping agents in the synthesis of AuNPs following the well-known Brust and Schiffrin procedure (see the Experimental Section).

The formation of nanoparticles was proven by the appearance of the gold plasmonic resonance absorption band centered around 520 nm (see Figure 5), accompanied by a color change to dark purple. The size of the nanoparticles was measured by DLS and TEM. The hydrodynamic diameter was measured by DLS; for AuNPs prepared using **1** as the capping agent, it was 4.2 ± 2 nm, while for nanoparticles stabilized with compound **4**, it was quite large, 15.0 ± 3.6 nm. TEM images of the nanoparticles with compound **1** showed a core radius of ca. 3 ± 2 nm (Figure 5),

dx.doi.org/10.1021/ic200792t |*Inorg. Chem.* 2011, 50, 8834–8849

Scheme 4. Schematization of the Synthetic Pathway To Decorate Silica Nanoparticles with Compound 8 and the TEM Image of Silica Nanoparticles Obtained

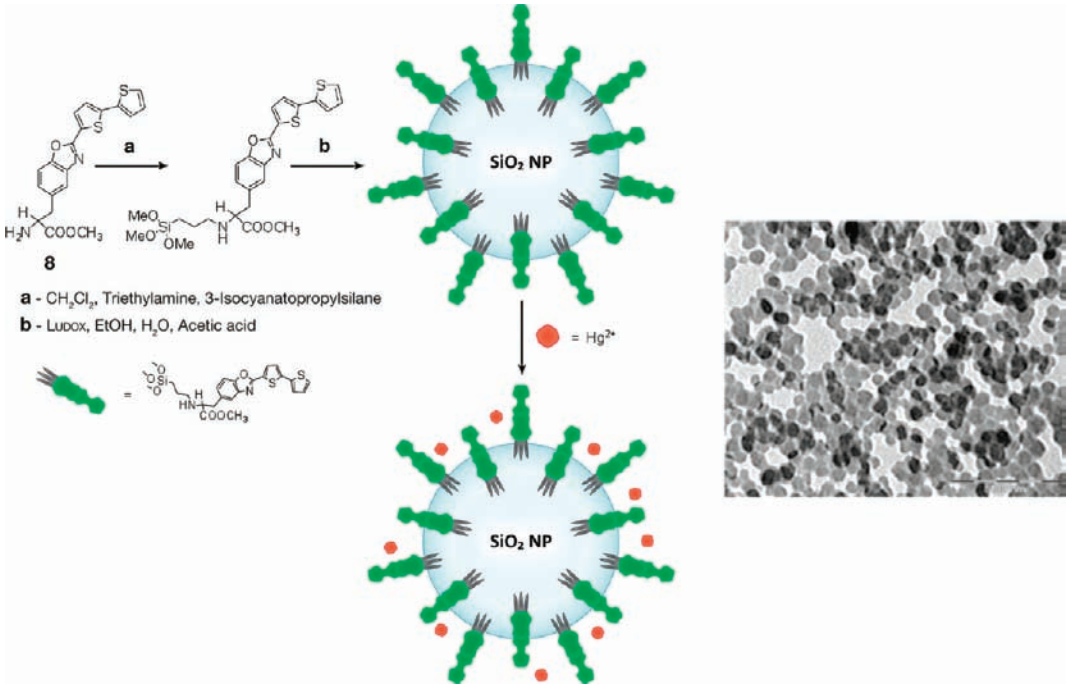

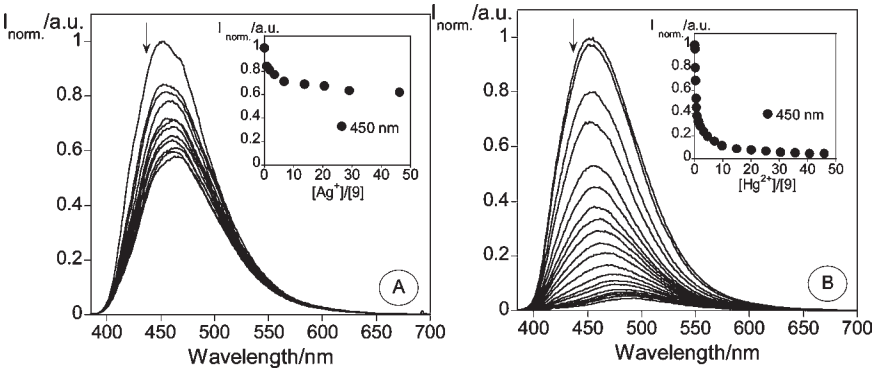

Figure 6. Spectrofluorimetric titration of silica nanoparticles functionalized at the surface with compound **9**, with increasing amounts of Ag^+ (A) and Hg^{2+} (B) in absolute ethanol. Inset: emission intensity at 450 nm as a function of $[Ag^+]/[9]$ (A) and as a function of $[Hg^{2+}]/[9]$ (B) ($[9] = 7.71 \times 10^{-6}$ M; $\lambda_{exc} = 368$ nm; $T = 298$ K).

while for the ones with compound **4**, we measured a diameter of 3.5 ± 2.5 nm. In both cases, the nanoparticles presented a polydispersed distribution, and this could be due to the steric hindrance of these compounds, which does not allow a perfect packing of the capping ligands on the surface, affecting the dimensional dispersion of the particles. Moreover, in the case of peptide **4**, some $\pi-\pi$-stacking interaction between the thienylbenzo[*d*]oxazole moieties could occur that, together with the possibility of forming different conformers on the AuNP surface, because of its longer flexible chain, could also induce particle aggregation.

In both cases, as far as emission properties are concerned, solutions of carefully washed nanoparticles redispersed in dichloromethane did not present any luminescence, and this complete quenching of the ligands proved their binding to the gold core. The quenching of the emission of a fluorophore linked to a AuNP is a typical effect; however, it is not always the case even for short spacers.[26]

Silica Nanoparticles Obtained by Surface Derivatization. The first strategy followed to combine the peptides with transparent silica nanoparticles was to derivatize **8** to **10** with an alkoxysilane group and then to anchor them to the surface of commercial Ludox silica nanoparticles (see Scheme 4).[27]

It was possible to determine an average number of 94, 29, and 27 molecules of **8**−**10**, respectively, per Ludox nanoparticle.[26] The profiles of the absorption and emission spectra of the derivatized nanoparticles were very similar to the ones of the free ligands, as expected because, on the one hand, the silica nanoparticles are totally transparent to the visible light and inert to electron-transfer processes[14] and, on the other hand, the

dx.doi.org/10.1021/ic200792t |*Inorg. Chem.* 2011, 50, 8834–8849

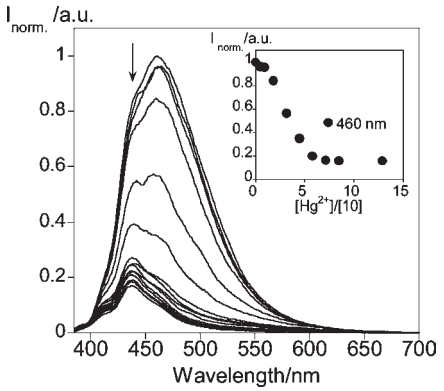

Figure 7. Spectrofluorimetric titration of silica nanoparticles functionalized at the surface with compound **10**, with increasing amounts of Hg^{2+} in dichloromethane. Inset: emission intensity at 460 nm as a function of $[Hg^{2+}]/[\mathbf{10}]$ ($[\mathbf{10}] = 2.14 \times 10^{-6}$ M; $\lambda_{exc} = 373$ nm; $T = 298$ K).

photophysics of these peptides is scarcely affected by the environment, as was previously discussed. DLS measurements of the new materials revealed diameters of 150 ± 10 nm for **8**, 665 ± 25 nm for **9**, and 6900 ± 25 nm for **10** decorated silica nanoparticles, demonstrating that the derivatization with the peptides induced their aggregation, which was more and more significant with an increase in the length of the peptide chain, a trend already observed also for AuNPs. For silica nanoparticles, the bonding of the peptides is expected to decrease their very negative surface potential, making them more prone to aggregation processes. The additional possibility of having intermolecular bonding among the molecules on the surface enhances this effect more and more.

We have explored the properties of these biocompatible species supported on different surfaces aiming to implement the design and realization of new fluorescent sensing species based on biomolecules for applications in biology and medicine. Toward this goal, we have also characterized the nanoparticles with peptides **8**−**10** using an instrumentation (NanoDrop)

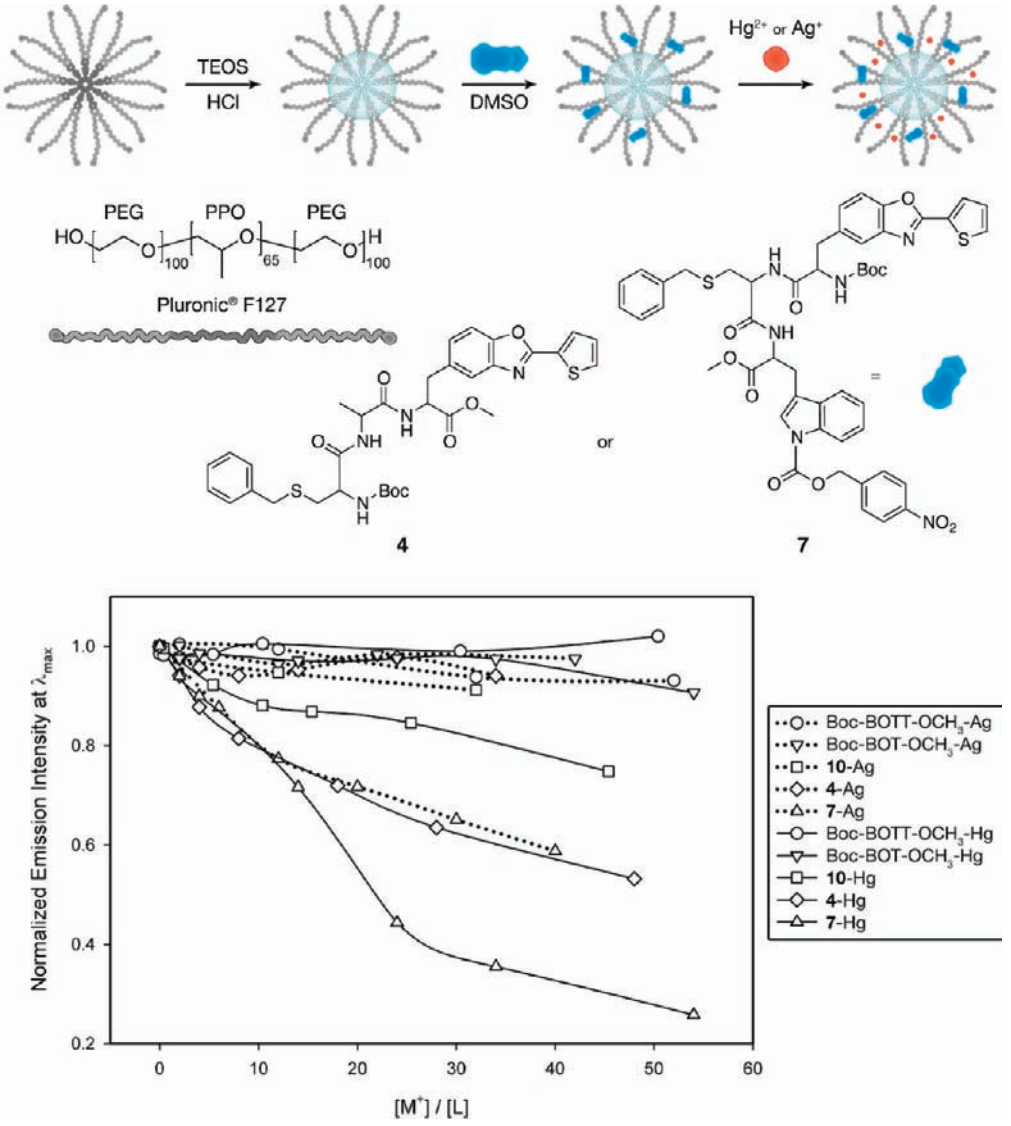

Figure 8. Schematization of the insertion of compound **4** or **7** in the outer layer of water-soluble CSNPs and titration profiles of the compounds in these conditions with increasing amounts of Ag^{+} and Hg^{2+}.

dx.doi.org/10.1021/ic200792t |*Inorg. Chem.* 2011, 50, 8834–8849

that allows the investigation of a few microliters of solution. In view of a possible introduction of these or similar systems as new proteomic platforms, the study of their behavior and reproducibility in very small samples is, in fact, particularly interesting. A total of 2 μL of a solution ca. 1.0×10^{-6} M of each nanoparticle batch was used in each experiment and titrated with increasing amounts of metal ions. In Figure S7 in the Supporting Information are reported the spectrofluorimetric titrations of compound **8** bound on the silica nanoparticles with Ag^+ (A) and Hg^{2+} (B). In both cases, the absorption spectra were not affected by the presence of the metal ion, while the fluorescence intensity was quenched by 20% and 80% upon the addition of Ag^+ or Hg^{2+}, respectively. An even higher interaction for Hg^{2+} ions was observed in the case of nanoparticles decorated with compound **9** (see Figure 6, panel B).

It is interesting to note that compounds **8** and **9** free in solution present an emission increase when titrated with Ag^+, while silica nanoparticles decorated with the same compounds undergo a nonnegligible emission quenching. This can probably be explained by hypothesizing the rise of cooperative effects in the complexation due to the short distance between the chromophores on the nanoparticles, yielding different stoichiometries and configurations. The results obtained with nanoparticles decorated with **10** are perfectly in line with those given by other systems. The addition of 5 equiv of Hg^{2+}, for example, caused an emission quenching of **10** of 90%, accompanied by a blue shift from 460 to 440 nm, as shown in Figure 7.

Moreover, upon the addition of Hg^{2+}, the nanoparticle size obtained via DLS measurements decreased from 6900 $\pm$ 25 to 57 $\pm$ 10 nm, indicating that the complexation of Hg^{2+} ions was able to induce a relevant decrease of the nanoparticle aggregation. A very similar result was recorded also for the system presenting compound **9** that passed from a diameter of 665 $\pm$ 25 to 46 $\pm$ 10 nm. These results, in our opinion, can possibly be attributed to reduction of the $\pi-\pi^*$ interaction between the (bi)thienylbenzo[*d*]oxazole chromophores when involved in complexation and/or to significant changes in the *Z* potential of the system.

All of the findings reported above indicate that when compounds **8** and **10** are bound on the surface of silica nanoparticles, they undergo a higher emission quenching with the same amount of Hg^{2+}, showing a higher sensitivity toward this metal ion.

Use of Core/Shell Water-Soluble Silica Nanoparticles. We have recently developed a new one-pot approach for the synthesis of water-soluble dye-doped silica core/shell nanoparticles (CSNPs) based on the preparation of micelles of Pluronic F127 in water.[28] The final material is a versatile multicompartment system characterized by a high water solubility, stability, and brightness. Most interestingly, we have also demonstrated the possibility of hosting in the outer PEG shell water-insoluble dyes, which are able to give rise to very efficient energy-transfer processes with the molecules hosted in the core, if present.[29] In an attempt to make the peptides operate in water, 10^{-4} M dimethyl sulfoxide solutions of **4**, **7**, and **10** were prepared. Small aliquots (1−10 μL) of these solutions were then added in 2.5 mL of a water dispersion containing 10^{-7} M CSNPs (Figure 8). Despite their poor solubility in pure water, in the presence of CSNPs, the peptides could be solubilized and thus revealed in this solvent by means of absorption and emission spectra perfectly matching the ones obtained for the same compounds in absolute ethanol. Moreover, a higher fluorescence anisotropy signal (>0.2) could be measured in the presence of CSNPs than in absolute ethanol, where the values were very close to zero. These data can be reasonably explained by the positioning of the peptides in the outer hydrophobic PEG shell of the nanoparticles, where they experience a reduced rotational freedom, as was already proven for analogous systems. We have then titrated with metal ions the ligand inside these complex structures, and compound **4** showed the most pronounced changes upon the addition of both Ag^+ and Hg^{2+} (Figure 8). It was also possible to calculate association constants for some of them and, in particular, for the complex of **4** with Hg^{2+}, it turned out to be smaller ($\log K = 3.80 \pm 0.20$) than that previously reported in solution ($\log \beta_{21} = 12.47 \pm 0.21$); however, it is important to note that in this case it was possible to perform all of the measurements in pure water. This last feature is particularly valuable because it makes these chemosensors suitable also for all of the applications that need water as a solvent such as medical and environmental ones.

CONCLUSIONS

A new family of bioinspired fluorescent peptide-based chemosensors, **2**−**4** and **7**−**10**, were successfully synthesized and characterized. All compounds had been studied by elemental analyses, MALDI-TOF-MS, IR, ^{1}H and ^{13}C NMR, UV−vis, and fluorescence spectroscopy.

These peptides showed, in general, high fluorescence quantum yields and high association constants with several metal ions of environmental and medical interest. We have then investigated their characteristics as fluorescent chemosensors in ethanol solutions and in the gas phase, using absorption and fluorescence spectroscopy and MALDI-TOF-MS to evidence the formation of the complexes. In all cases, the strongest affinity and sensitivity were observed in the presence of the heavy and pollutant Hg^{2+} ions. The results showed that the insertion of an alanine residue (natural amino acid) on going from **2** to **4** and from **9** to **10** increased the affinity toward Hg^{2+} ions, which could probably be explained by the higher flexibility of the longer ligands. This is a very interesting result in view of the design of a second generation of more efficient bioinspired chemosensors.

Aiming to explore new possibilities for the design and realization of fluorescent sensing species based on biomolecules for applications in biology and medicine, we have bound our active moieties on different surfaces and then characterized these new materials. The use of supported molecules is generally a fundamental step in order to build sensing devices, and, in general, this opens up many new possibilities for applications. We have, therefore, verified whether the characteristics and properties of our materials could be maintained or even improved when included in a more complex architecture.

These ligands were first bound on the surface of AuNPs. In particular, compounds **1** and **4** were used as stabilizing agents in the well-known Brust and Schiffrin synthetic strategy to successfully obtain stable AuNPs. As in most cases when fluorophores are linked on the surface of AuNPs, the fluorescence signal of both **1** and **4** was completely quenched and did not undergo to any changes by the addition of all of the metal ions studied; this unfortunately prevented their possible investigation as chemosensors.

To overcome this important drawback, we decided to investigate more inert materials as possible supports for our ligands and, in particular, silica. We therefore derivatize peptides **8**−**10** with a suitable anchoring group, namely, triethoxysilane, to covalently link them to the surface of commercial Ludox nanoparticles of 15 $\pm$ 3 nm diameter. The systems were

dx.doi.org/10.1021/ic200792t |*Inorg. Chem.* 2011, 50, 8834–8849

successfully obtained and because of the inert nature of silica, as expected, the nanoparticles were highly luminescent, in line with the behavior of the peptides in solution. These new hybrid systems were able to efficiently complex Hg^{2+} and Ag^{+} ions, with a concomitant quenching of the fluorescence intensity. Moreover, when compounds **8** and **9** were bound on the surface of silica nanoparticles, they underwent a higher emission quenching with the same amount of Hg^{2+}, showing higher sensitivity toward this metal ion. This can be attributed only to new positive cooperative effects in the complexation rising between the ligands due to their close vicinity on the nanoparticles. We have already demonstrated, in fact, that this architecture can yield enhanced sensitivity because the cooperativity of two or more neighboring units in each binding event[15b,e] can substantially increase the efficiency of the complexation and it can also contribute to inducing collective responses of more than one active unit per interacting metal ion.[15b,26]

Finally, we have shown the successful vehiculation of some of the chemosensors in study in water, despite their very poor solubility in this solvent, inserting them in the outer PEG shell of silica core/PEG shell nanoparticles recently developed in our laboratories. In these conditions, compound **4** was also able to signal the presence of Hg^{2+} and Ag^{+} ions, confirming that this is an efficient strategy to enable this family of bioinspired chemosensors to work in water, greatly enlarging the possibilities offered by these species. Further experiments to obtain signal amplification effects inserting dyes in the silica core of these nanoparticles are in due course in our laboratories.

■ ASSOCIATED CONTENT

Supporting Information. Spectrophotometric and spectrofluorimetric titrations of **2**−**4** and **7**−**10** with Hg^{2+} in absolute ethanol and **10** in the presence of Ag^{+}, spectrofluorimetric titrations of compounds **3**, **4**, **7**, and **10** in the presence of Fe^{3+} in absolute ethanol, spectrofluorimetric titration of silica nanoparticles of compound **8** with the addition of Ag^{+} and Hg^{2+} in absolute ethanol, selectivity studies of compounds **3**, **4**, **7**, and **10** for metal ions, and TEM images of AuNP and silica nanoparticles with compounds **4** and **9**. This material is available free of charge via the Internet at http://pubs.acs.org.

■ AUTHOR INFORMATION

Corresponding Authors

*E-mail: spc@quimica.uminho.pt (S.P.G.C.), luca.prodi@unibo.it (L.P.), clodeiro@uvigo.es (C.L.).

■ ACKNOWLEDGMENT

We thank Xunta de Galiza (Spain) for Project 09CSA043383PR (Biomedicine) and the University of Vigo for Projects INOU UVIGO/VICOU/K914-122P64702/2009 and UVIGO/VICOU/K912-122P64702/2009. Thanks go to the FCT-MCTES/FEDER (Portugal) through National Project PDTC/QUI/66250/2006 (FCOMP-01-0124-FEDER-007428). Financial support from the program NanoSci-E+ (financed project "INOFEO") and from Fondazione Cassa di Risparmio in Bologna is also gratefully acknowledged. E.O. thanks FCT/Portugal for a postdoctoral grant (SFRH/BPD/72557/2010) and Fundação Calouste Gulbenkian for the Prize 2008 in Excellence in Research (Estímulo à Creatividade e a Qualidade na Actividade de Investigação). C.L. and J.L.C. thank Xunta de Galicia for the Isidro Parga Pondal Research Program. C.L. thanks the Royal Society of Chemistry for a Journal Grant for International Authors 2008. The NMR spectrometer Bruker Avance III 400 is part of the National NMR Network and was purchased within the framework of the National Program for Scientific Re-equipment [Contract REDE/1517/RMN/2005 with funds from POCI 2010 (FEDER) and FCT].

■ DEDICATION

‖In honor of the 100th years of the Portuguese Society of Chemistry

■ REFERENCES

(1) (a) Czarnik, A. W. *Acc. Chem. Res.* **1994**, *21*, 302–308. (b) Lodeiro, C.; Pina, F. *Coord. Chem. Rev.* **2009**, *253*, 1353–1383. (c) Lodeiro, C.; Capelo, J. L.; Mejuto, J. C.; Oliveira, E.; Santos, H. M.; Pedras, B.; Nuñez, C. *Chem. Soc. Rev.* **2010**, *39*, 2948–2976.

(2) (a) Ulijn, R. V.; Smith, A. M. *Chem. Soc. Rev.* **2008**, *37*, 664–675. (b) Cavalli, S.; Albericio, F.; Kros, A. *Chem. Soc. Rev.* **2010**, *39*, 241–263. (c) Sawada, T.; Takahashi, T.; Mihara, H. *J. Am. Chem. Soc.* **2009**, *131*, 14434–14441.

(3) (a) Guzow, K.; Milewska, M.; Wróblewski, D.; Gieldón, A.; Wiczk, W. *Tetrahedron* **2004**, *60*, 11889–11894. (b) Milewska, M.; Skwierawska, A.; Guzow, K.; Szmigiel, D.; Wiczk, W. *Inorg. Chem. Commun.* **2005**, *8*, 947–950.

(4) Joshi, B. P.; Cho, W.-M.; Kim, J.; Yoon, J.; Lee, K.-H. *Bioorg. Med. Chem. Lett.* **2007**, *17*, 6425–6429.

(5) Zheng, Y.; Cao, X.; Orbulescu, J.; Konka, V.; Andreopoulos, F. M.; Phan, S. M.; Leblanc, R. M. *Anal. Chem.* **2003**, *75*, 1706–1712.

(6) Li, Y.; Yang, M. *J. Am. Chem. Soc.* **2005**, *127*, 3527–3530.

(7) McGrath, M. E.; Sprengeler, P. A.; Hill, C. M.; Martichonok, V.; Cheung, H.; Somoza, J. R.; Palmer, J. T.; Janc, J. W. *Biochemistry* **2003**, *42*, 15018–15028.

(8) (a) Prodi, L. *New J. Chem.* **2005**, *29*, 20–31. (b) Bonacchi, S.; Genovese, D.; Juris, R.; Montalti, M.; Prodi, L.; Rampazzo, E.; Zaccheroni, N. *Angew. Chem., Int. Ed.* **2011**, *50*, 2–13. (c) Bonacchi, S.; Genovese, D.; Juris, R.; Montalti, M.; Prodi, L.; Rampazzo, E.; Sgarzi, M.; Zaccheroni, N. *Top. Curr. Chem.* **2011**, *300*, 93–138.

(9) Bonacchi, S.; Genovese, D.; Juris, R.; Mancin, F.; Montalti, M.; Prodi, L.; Rampazzo, E.; Zaccheroni, N. In *Handbook of Porphyrin Science*; Kadish, K. M., Smith, K. M., Guilard, R., Eds.; World Scientific: New York, 2010; Vol. 12, Chapter 5.

(10) (a) Boisselier, E.; Astruc, D. *Chem. Soc. Rev.* **2009**, *38*, 1759–1782. (b) Aili, D.; Stevens, M. M. *Chem. Soc. Rev.* **2010**, *39*, 3358–3370. (c) Klajn, R.; Stoddart, J. F.; Grzybowski, B. A. *Chem. Soc. Rev.* **2010**, *39*, 2203–2237. (d) Bunz, U. H. F.; Rotello, V. M. *Angew. Chem., Int. Ed.* **2010**, *49*, 3268–3279. (e) Giljohann, D. A.; Seferos, D. S.; Daniel, W. L.; Massich, M. D.; Patel, P. C.; Mirkin, C. A. *Angew. Chem., Int. Ed.* **2010**, *49*, 3280–3294. (f) Liu, S. Q.; Tang, Y. Z. *J. Mater. Chem.* **2010**, *20*, 24–35.

(11) (a) Vial, St.; Mansuy, C.; Sagan, S.; Irinopoulou, T.; Burlina, F.; Boudou, J.-P.; Chassaing, G.; Lavielle, S. *ChemBioChem* **2008**, *9*, 2113–2119. (b) Knecht, M. R.; Scthi, M. *Anal. Bioanal. Chem.* **2009**, *394*, 33–46. (c) Wang, Z.; Ma, L. *Coord. Chem. Rev.* **2009**, *253*, 1607–1618.

(12) (a) Montalti, M.; Prodi, L.; Zaccheroni, N.; Beltrame, M.; Morotti, T.; Quici, S. *New J. Chem.* **2007**, *31*, 102–108. (b) Montalti, M.; Zaccheroni, N.; Prodi, L.; O'Reilly, N.; James, S. L. *J. Am. Chem. Soc.* **2007**, *129*, 2418–2419. (c) Montalti, M.; Prodi, L.; Zaccheroni, N.; Battistini, G. *Langmuir* **2004**, *20*, 7884–7886. (d) Montalti, M.; Prodi, L.; Zaccheroni, N.; Baxter, R.; Teobaldi, G.; Zerbetto, F. *Langmuir* **2003**, *19*, 5172–5174.

(13) He, X.; Liu, H.; Li, Y.; Wang, S.; Li, Y.; Wang, N.; Xiao, J.; Xu, X.; Zhu, D. *Adv. Mater.* **2005**, *17*, 2811–2815.

(14) (a) Burns, A.; Ow, H.; Wiesner, U. *Chem. Soc. Rev.* **2006**, *35*, 1028–1042. (b) Wang, L.; Wang, K. M.; Santra, S.; Zhao, X. J.; Hilliard, L. R.; Smith, J. E.; Wu, J. R.; Tan, W. H. *Anal. Chem.* **2006**, *78*, 646–654. (c) Yong, K. T.; Roy, I.; Swihart, M. T.; Prasad, P. N. *Mater. Chem.* **2009**, *19*, 4655–4672.

(15) (a) Burns, A.; Sengupta, P.; Zedayko, T.; Baird, B.; Wiesner, U. *Small* **2006**, *2*, 723–726. (b) Arduini, M.; Rampazzo, E.; Manicn, F.; Tecilla, P.; Tonellato, U. *Inorg. Chim. Acta* **2007**, *360*, 721–727. (c) Doussineau, T.; Shulz, A.; Lapresta-Fernandez, A.; Moro, A.; Körsten, S.; Trupp, S.; Mohr, G. J. *Chem.—Eur. J.* **2010**, *16*, 10290–10299. (d) Montalti, M.; Prodi, L.; Zaccheroni, N. *J. Mater. Chem.* **2005**, *15*, 2810–2814. (e) Bonacchi, S.; Rampazzo, E.; Montalti, M.; Prodi, L.; Zaccheroni, N.; Mancin, F.; Teolato, P. *Langmuir* **2008**, *24*, 8387–8392. (f) Zanarini, S.; Rampazzo, E.; Ciana, D. L.; Marcaccio, M.; Marzocchi, E.; Montalti, M.; Paolucci, F.; Prodi, L. *J. Am. Chem. Soc.* **2009**, *131*, 2260–2267. (g) Seo, S.; Lee, H. Y.; Park, M.; Lim, J. M.; Kang, D.; Yoon, J.; Jung, J. H. *Eur. J. Inorg. Chem.* **2010**, 843–847.

(16) Si, S.; Kotal, A.; Mandal, T. K. *J. Phys. Chem. C* **2007**, *111*, 1248–1255.

(17) (a) Costa, S. P. G.; Oliveira, E.; Lodeiro, C.; Raposo, M. M. M. *Sensors* **2007**, *7*, 2096–2114. (b) Costa, S. P. G.; Oliveira, E.; Lodeiro, C.; Raposo, M. M. M. *Tetrahedron Lett.* **2008**, *49*, 5258–5261. (c) Oliveira, E.; Costa, S. P. G.; Raposo, M. M. M.; Lodeiro, C. *Inorg. Chim. Acta* **2011**, *366*, 154–160.

(18) (a) Chen, X.; Nam, S.-W.; Jou, M.; Kim, Y.; Kim, S.-J.; Park, S.; Yoon, J. *Org. Lett.* **2008**, *10*, 5235–5238. (b) Nolan, E. M.; Lippard, S. J. *Chem. Rev.* **2008**, *108*, 3443–3480. (c) Tamayo, A.; Pedras, B.; Lodeiro, C.; Escriche, L.; Casabó, J.; Capelo, J. L.; Covelo, B.; Kivekas, R.; Sillampaa, R. *Inorg. Chem.* **2007**, *46*, 7818–7826. (d) Mameli, M.; Lippolis, V.; Caltagirone, C.; Capelo, J. L.; Nieto-Faza, O.; Lodeiro, C. *Inorg. Chem.* **2010**, *49*, 8276–8286.

(19) (a) Rocha, A.; Marques, M. M. B.; Lodeiro, C. *Tetrahedron Lett.* **2009**, *50*, 4930–4933. (b) Swamy, K. M. K.; Kim, H. N.; Soh, J. H.; Kim, Y.; Kim, S.-J.; Yoon, J. *Chem. Commun.* **2009**, 1234–1236. (c) Park, C. S.; Lee, J. Y.; Kang, E.-J.; Lee, J.-E.; Lee, S. S. *Tetrahedron Lett.* **2009**, *50*, 671–675. (d) Tamayo, A.; Oliveira, E.; Covelo, B.; Casabó, J.; Escriche, Ll.; Lodeiro, C. *Z. Anorg. Allg. Chem.* **2007**, *633*, 1809–1814.

(20) (a) Brust, M.; Fink, J.; Bethell, D.; Schiffrin, D. J.; Kiely, C. *J. Chem. Soc., Chem. Commun.* **1994**, 801–802. (b) Brust, M.; Fink, J.; Bethell, D.; Schiffrin, D. J.; Kiely, C. *J. Chem. Soc., Chem. Commun.* **1995**, 1655–1656.

(21) Credi, A.; Prodi, L. *Spectrochim. Acta, Part A* **1998**, *54*, 159–170.

(22) (a) Berlman, I. B. *Handbook of Fluorescence Spectra of Aromatic Molecules*, 2nd ed.; Academic Press: New York, 1971. (b) Montalti, M.; Credi, A.; Prodi, L.; Gandolfi, M. T. *Handbook of Photochemistry*, 3rd ed.; Taylor & Francis: Boca Raton, FL, 2006.

(23) (a) Friggeri, A.; Montalti, M.; Dolci, L. S.; Prodi, L.; Zaccheroni, N.; Stuart, M. C. A.; van Bommel, K. J. C. *Langmuir* **2006**, *22*, 2299–2303. (b) Montalti, M.; Prodi, L.; Zaccheroni, N.; Battistini, G.; Marcuz, S.; Mancin, F.; Rampazzo, E.; Tonellato, U. *Langmuir* **2006**, *22*, 5877–5881.

(24) Harris, D. C. *Quantitative Chemical Analysis*, 6th ed.; W. H. Freeman and Cia: New York, 2002.

(25) *SPECFIT/32 Global Analysis System*, version 3.0; Spectrum Software Associates: Malborough, MA.

(26) Battistini, G.; Cozzi, P. G.; Jalkanen, J.-P.; Montalti, M.; Prodi, L.; Zaccheroni, N.; Zerbetto, F. *ACS Nano* **2008**, *2*, 77–84.

(27) Montalti, M.; Prodi, L.; Zaccheroni, N.; Falini, G. *J. Am. Chem. Soc.* **2002**, *124* (45), 13540–13546.

(28) Zanarini, S.; Rampazzo, E.; Bonacchi, S.; Juris, R.; Marcaccio, M.; Montalti, M.; Paolucci, F.; Prodi, L. *J. Am. Chem. Soc.* **2009**, *131*, 14208–14209.

(29) Rampazzo, E.; Bonacchi, S.; Juris, R.; Montalti, M.; Genovese, D.; Zaccheroni, N.; Prodi, L.; Rambaldi, D. C.; Zattoni, A.; Reschiglian, P. *J. Phys. Chem. B* **2010**, *114*, 14605–14613.